Supporting Information

Supramolecular Assembly of Amphiphilic Platinum(II) Schiff Base Complexes: Diverse Spectroscopic Changes and Nanostructures through Rational Molecular Design and Solvent Control

Huilan Zhang,[a,b] Michael Ho-Yeung Chan,[b] Jonathan Lam,[b] Ziyong Chen,[b] Ming-Yi Leung,[b] Eric Ka-Ho Wong,[b] Lixin Wu*[a] and Vivian Wing-Wah Yam*[a,b]

[a]State Key Laboratory of Supramolecular Structure and Materials and College of Chemistry, Jilin University, Changchun 130012, P. R. China.

[b]Institute of Molecular Functional Materials and Department of Chemistry, The University of Hong Kong, Pokfulam Road, Hong Kong SAR, P. R. China.

Photophysical Measurements and Instrumentation

^{1}H NMR and ^{13}C{^{1}H} NMR spectra were obtained on a Bruker DRX 500 (500 MHz) spectrometer at 298 K with chemical shifts reported relative to tetramethylsilane (Me_4Si). 2D ^{1}H–^{1}H NOESY NMR spectra were recorded on a Bruker DRX 600 (600 MHz) spectrometer at 298 K with chemical shifts reported relative to tetramethylsilane (Me_4Si). All MALDI-TOF mass spectra were recorded on a Autoflex speed TOF/TOF mass spectrometer. Elemental analysis was carried out on a Vario micro cube analyzer from Elementar. The single crystal structure was obtained on a R-AXIS RAPID X-ray single crystal diffractometer. UV−Vis absorption spectra were recorded using a Varian Cary 50 UV−vis spectrophotometer. Steady-state excitation and emission spectra at room temperature were obtained on an Edinburgh Instruments FS5 spectrofluorometer. Time-resolved photoluminescence decay traces and lifetimes at room temperature were obtained on an Edinburgh Instruments FLS1000 spectrofluorometer. The temperature-dependent UV−vis absorption spectra were obtained using a Varian Cary S-1 50 UV−vis spectrophotometer equipped with a Varian Cary single cell peltier thermostat. Dynamic light scattering (DLS) experiments were performed on a Malvern Zetasizer NanoZS instrument. TEM images were obtained with a JEM-2100F electron microscope operating at 200 kV. SEM images were obtained with a Hitachi SU8020 at 3 kV. Atomic force microscope (AFM) measurements were carried out on a Bruker FastScan atomic force

microscope. X-Ray diffraction (XRD) data were recorded on a Rigaku X-ray diffractometer using Cu-Kα radiation at a wavelength of 1.542 Å.

Computational Details

All calculations were performed using the Gaussian16 suite of programs[1] on research computing facilities offered by Information Technology Services at the University of Hong Kong.

Geometries for the monomer **7** were optimized in dimethyl sulfoxide (DMSO) using the Perdew-Burke-Ernzerhof parameter-free hybrid functional[2,3] (PBE0) in conjunction with the Solvation Model based on Density (SMD).[4] This was followed by the calculation of vibrational frequencies at the same level of theory to verify that each is a minimum (NIMAG=0) on the potential energy surface. The Stuttgart effective core potentials (ECPs) and the associated basis set were used to describe platinum[5] with an f-type polarization function ($\zeta = 0.993$),[6] whereas the remainder of the complex was described using the 6-31G(d,p) basis set.[7–10] These calculations were performed on the ground state (S_0) and lowest triplet excited state (T_1) of **7**.

To reflect the change in conditions for the case of the dimer $\mathbf{7}_2$, the SMD solvent was replaced with water, retaining the use of the PBE0 functional. Furthermore, platinum centers were described using the Stuttgart ECPs and the associated basis set, with two f-type polarization functions (ζ = 0.70 and 0.14).[11] All remaining atoms were described at the PBE0/6-31G(d,p) level of theory, as in the monomer case. Using the crystal structure as an initial estimate, both S_0 and T_1 states of $\mathbf{7}_2$ were fully optimized in this way.

Time-dependent DFT (TDDFT)[12–14] calculations were performed on the ground state (S_0) geometry of **7** and $\mathbf{7}_2$. The resulting Franck-Condon absorption bands (singlet–singlet transitions, 50 states) were computed to simulate UV−vis spectra using the Multiwfn package.[15] In principle, emission maximal wavelength should be simulated using the optimized T_1 state geometry. However, due to the poor performance of TDDFT in describing the triplet states of transition metal complexes at their optimized T_1 structure, the phosphorescence emission energy is usually calculated at the S_0 state geometry to better correlate with experimental results.[16] As such, the emission energies of **7** and $\mathbf{7}_2$ were also calculated using their S_0 structures.[16] Non-covalent interactions were calculated with NCIplot,[17–19] which makes use of the electron density and its gradient at critical points between molecules, and the resulting isosurfaces were modeled using Visual Molecular Dynamics (VMD)

1.9.3.[20] NCI plot depicts non-covalent interactions as an isosurface plot, using blue for strong attractive interactions, green for weak van der Waals interactions and red for strong repulsive interactions. Cartesian coordinates of the S_0 and T_1 states of **7** and $\mathbf{7}_2$ in their optimized geometries are given in **Tables S4–S7**. All DFT and TDDFT calculations were performed with a pruned (99,590) grid for numerical integration.

Notably, we have observed that the dimer structure exhibits an energetically lower-lying absorption band (λ_{abs} = 525 nm) compared to that of the monomer (λ_{abs} = 503 nm, see Table S8). However, this lower-lying band is not visible in the calculated dimer spectrum due to its very small oscillator strength (f = 0.000). The optimized dimer possesses approximate C_i point group symmetry, leading to orbitally forbidden HOMO→LUMO transition ($A_g \rightarrow A_g$). Nevertheless, the intensity of this low-energy band can be significantly enhanced by breaking the symmetry of the dimer. For instance, by slightly tilting the O^N^N^O plane of one monomer with respect to the other, the oscillator strength of the HOMO→LUMO transition of distorted $\mathbf{7}_2$ is increased to 0.019 (Figure S21c). Comparing the simulated absorption spectra of **7** and $\mathbf{7}_2$, a significant enhancement of lower-energy absorption tail (λ_{abs} = 525 nm) of the distorted dimer $\mathbf{7}_2$ is observed (Figure S21d). Under experimental conditions, this approximate symmetry can be broken by molecular vibrations and thermal distortions in solution. It is important to note that this approximate symmetry is absent in higher-order aggregates such as trimers and tetramers. This is consistent with the red shift of the UV–vis absorption band of **4** observed experimentally upon increasing water content (Figures S21e). Further deconvolution analysis has been carried out, in which a red shift and emergence of new deconvoluted lower-energy band in 20 % water–DMSO (v/v) is observed (Figures S21f and S21g), suggestive of the possible formation of dimer, trimer and oligomer in the self-assembly of the complex. Our computational results are consistent with the experimentally observed enhancement in the low-energy absorption band during the self-assembly process.

Temperature-dependent Nucleation–Elongation Model in Curve Fitting

Temperature-dependent nucleation–elongation model[21] was developed by Meijer and coworkers and has been applied to fit the experimental data in the variable temperature UV–vis spectroscopic studies for complexes **2–6** in DMSO–water mixtures. All cooling curves obtained are

performed at a slow cooling rate of 0.5 K min^{-1} to ensure that the self-assembly processes were under thermodynamic control.[21]

Nucleation–Elongation Model

The nucleation and elongation regimes are governed by the following equations (1) and (2) respectively.

$$\phi_n = K_a^{1/3} exp\left[\left(2/3\, K_a^{-1/3} - 1\right)\frac{h_e}{RT_e^2}(T - T_e)\right] \quad (1)$$

$$\phi_n = \phi_{SAT}\left(1 - exp\left[-\frac{h_e}{RT_e^2}(T - T_e)\right]\right) \quad (2)$$

ϕ_n is the degree of aggregation, and ϕ_{SAT} is a factor introduced to the equation such that ϕ_n/ϕ_{SAT} does not exceed unity. h_e is the molecular enthalpy released due to non-covalent interactions during elongation process, T_e is the elongation temperature, K_a is the dimensionless equilibrium constant of the nucleation process at T_e and R is the universal gas constant.

Moreover, the number-averaged degree of polymerization averaged over all active species in the elongation regime at a temperature T, $\langle N_n \rangle$, is given by equation (3) below:

$$\langle N_n(T) \rangle = \frac{1}{\sqrt{K_a}}\frac{\phi_n}{\phi_{SAT} - \phi_n} \quad (3)$$

Whereas the number-averaged degree of polymerization averaged over all active nucleated species at T_e, and is given by equation (4) as follows.

$$\langle N_n(T_e) \rangle = \frac{1}{\sqrt[3]{K_a}} \quad (4)$$

Experimental Section

Materials and Reagent: Potassium tetrachloroplatinate(II) ($K_2[PtCl_4]$) (Chem. Pur., 98 %), copper(I) iodide (CuI), tetrakis(triphenylphosphine) palladium(0) ($Pd(PPh_3)_4$), 2-hydroxybenzaldehyde and 1-bromo-3,5-dimethoxybenzene were purchased from Energy Chemical Co, Ltd. Dimethyl sulfoxide (DMSO), tetrahydrofuran (THF), dichloromethane (DCM), diisopropylamine (DIPA) and sodium sulphate (Na_2SO_4) were the products of Beijing Chemical Reagent Company. All commercially available reagents were of analytical grade and were used as

received. All solvents were purified and distilled using standard procedures before use. 2-hydroxy-5-iodobenzaldehyde[22], (C≡C-Ph-$(OTEG)_2$)[23], benzene-1,2-diamine with different oxyalkyl chain[24] and triethylene glycol-pendant[25] and **L1**–**L6**[26] were synthesized according to previously reported literature procedures.

Sample preparation

The photophysical data including the UV–vis absorption and emission spectra, lifetime and photoluminescence quantum yields of complexes **1**–**6** were performed in degassed DMSO solutions at the concentration of ~10^{-5} M at 298 K. The photoluminescence decay traces of **1**–**5** were recorded at 654 nm and the photoluminescence decay trace of **6** was recorded at 641 nm, respectively. Solvatochromic properties of complexes **2**–**6** were measured under degassed condition at the concentration of ~10^{-5} M at 298 K. The concentration-dependent UV–vis absorption and emission spectra of complex **6** in water and concentration-dependent UV–vis absorption of complexes **2**–**6** in DMSO solutions were obtained under ambient conditions at 298 K. The UV–vis absorption, emission, excitation spectra and time-resolved photoluminescence decay traces of complexes **2**–**6** in mixed solvent compositions (DMSO–water) were measured under ambient conditions at the concentration of ~10^{-5} M at 298 K after standing for 40 mins. The temperature-dependent UV–vis absorption and emission spectra of complexes **2**–**6** were performed under ambient conditions at the concentration of ~10^{-5} M. The samples for TEM and AFM measurements were prepared by drop-casting the solutions onto the carbon grid and silicon wafer and allowing the remaining solvent to evaporate. Samples for XRD experiments were prepared by filtrating by 0.45 μL filter membrane with higher concentration solutions followed by drying at room temperature, and this procedure was repeated 2–3 times to accumulate enough samples for obtaining XRD signals.

Synthesis

Experimental Procedures

PtL1. A solution of the Schiff base ligand **L1** (85.5 mg, 0.12 mmol) and K_2CO_3 (50.0 mg, 0.36 mmol) was stirred for about 0.5 h in dry THF under nitrogen at 60 ºC. Then, a DMSO (2 ml) solution of K_2PtCl_4 (50.0 mg, 0.12 mmol) was added to the reaction mixture, which was continuously stirred for 3 days under nitrogen at 60 ºC. The reaction mixture was extracted with CH_2Cl_2 and washed

with water several times. The organic layer was further washed with brine. The residue after solvent evaporation was recrystallized using dichloromethane/methanol to give a red solid. Yield: 61.4 mg (57 %). ^{1}H NMR (500 MHz, $CDCl_3$, 298 K) δ / ppm = 8.46 (s, 2H, –NCH–), 7.85 (d, J = 2.2 Hz, 2H, phenyl), 7.63 (dd, J = 8.9, 2.2 Hz, 2H, phenyl), 7.25 (s, 2H, phenyl), 7.14 (d, J = 8.9 Hz, 2H, phenyl), 4.12 (s, 4H, –OCH_2–), 1.91 (m, 4H, –CH_2–), 1.28 (s, 4H, –CH_2–), 1.07 (t, J = 7.4 Hz, 6H, –CH_3). Elemental analysis calcd (%) for $C_{28}H_{28}N_2O_4I_2Pt$: C 37.14, H 3.12, N 3.09. Found: C 37.30, H 3.41, N 3.01. MALDI-TOF MS: m/z = 904.32 $[M]^+$.

PtL2. The procedure was similar to that described for the synthesis of **PtL1**, except Schiff base ligand **L2** (92.2 mg, 0.12 mmol) was used in place of **L1**. The crude product was recrystallized using dichloromethane/methanol to give a red solid. Yield: 70.6 mg (61 %). ^{1}H NMR (500 MHz, $CDCl_3$, 298 K) δ / ppm = 8.33 (s, 2H, –NCH–), 7.74 (d, J = 2.2 Hz, 2H, phenyl), 7.65 (dd, J = 9.1, 2.2 Hz, 2H, phenyl), 7.12 (s, 2H, phenyl), 7.07 (d, J = 9.1 Hz, 2H, phenyl), 4.04 (t, J = 6.4 Hz, 4H, –OCH_2–), 1.86 (m, 4H, –CH_2–), 1.53 (m, 4H, –CH_2–), 1.42 (m, 8H, –CH_2–), 0.98 (t, J = 6.9 Hz, 6H, –CH_3); ^{13}C{^{1}H} NMR (125 MHz, $CDCl_3$, 298 K) δ / ppm = 163.97, 149.15, 145.87, 142.77, 141.71, 137.92, 124.60, 124.30, 98.39, 69.68, 31.69, 29.16, 25.72, 22.68, 14.12. Elemental analysis calcd (%) for $C_{32}H_{36}N_2O_4I_2Pt$: C 39.97, H 3.77, N 2.91. Found: C 40.19, H 3.88, N 3.04. MALDI-TOF MS: m/z = 961.04 $[M]^+$.

PtL3. The procedure was similar to that described for the synthesis of **PtL1**, except Schiff base ligand **L3** (90.0 mg, 0.12 mmol) was used in place of **L1**. The crude product was recrystallized using dichloromethane/methanol to give a red solid. Yield: 76.3 mg (62 %). ^{1}H NMR (500 MHz, $CDCl_3$, 298 K) δ / ppm = 8.27 (s, 2H, –NCH–), 7.71 (d, J = 2.1 Hz, 2H, phenyl), 7.64 (dd, J = 8.8, 2.1 Hz, 2H, phenyl), 7.13 (s, 2H, phenyl) 7.06 (d, J = 2.1 Hz, 2H, phenyl), 4.02 (s, 4H, –OCH_2–), 1.87 (s, 4H, –CH_2–), 1.52 (m, 4H, –CH_2–), 1.37 (m, 16H, –CH_2–), 0.94 (t, J = 7.2 Hz, 6H, –CH_3); ^{13}C{^{1}H} NMR (125 MHz, $CDCl_3$, 298 K) δ / ppm = 163.44, 148.66, 145.33, 142.57, 141.53, 137.35, 124.20, 124.13, 98.05, 69.51, 41.02, 31.95, 29.62, 29.40, 29.26, 26.06, 22.78, 14.23. Elemental analysis calcd (%) for $C_{36}H_{44}N_2O_4I_2Pt$: C 42.49, H 4.36, N 2.75. Found: C 42.26, H 4.43, N 2.56. MALDI-TOF MS: m/z = 1017.42 $[M]^+$.

PtL4. The procedure was similar to that described for the synthesis of **PtL1**, except Schiff base ligand **L4** (112 mg, 0.12 mmol) was used in place of **L1**. The crude product was recrystallized using dichloromethane/methanol to give a red solid. Yield: 81.6 mg (60 %). ^{1}H NMR (500 MHz, $CDCl_3$,

298 K) δ / ppm = 8.13 (s, 2H, –NCH–), 7.59 (d, J = 8.9, 2.0 Hz, 2H, phenyl), 7.43 (d, J = 2.0 Hz, 2H, phenyl), 6.97 (d, J = 8.9 Hz, 2H, phenyl), 6.91 (s, 2H, phenyl), 3.89 (t, J = 6.7 Hz, 4H, –OCH_2–), 1.79 (m, 4H, –CH_2–), 1.34 (m, 36H, –OCH_2–), 0.92 (t, J = 7.1 Hz, 6H, –CH_3); $^{13}C\{^1H\}$ NMR (125 MHz, $CDCl_3$, 298 K) δ / ppm = 163.78, 148.94, 145.62, 142.83, 141.65 137.65, 124.53, 124.29, 98.25, 69.71, 32.14, 29.93, 29.61, 26.22, 22.89, 14.32. Elemental analysis calcd (%) for $C_{44}H_{60}N_2O_4I_2Pt$: C 46.77, H 5.35, N 2.48. Found: C 46.56, H 5.28, N 2.69. MALDI-TOF MS: m/z = 1129.67 $[M]^+$.

PtL5. The procedure was similar to that described for the synthesis of **PtL1**, except Schiff base ligand **L2** (124 mg, 0.12 mmol) was used in place of Schiff base ligand **L1**. The crude product was recrystallized using dichloromethane/methanol to give a red solid. Yield: 90.6 mg (61 %). ^1H NMR (500 MHz, $CDCl_3$, 298 K) δ / ppm = 8.19 (s, 2H, –NCH–), 7.63 (d, J = 2.1 Hz, 2H, phenyl), 7.59 (dd, J = 9.0, 2.1 Hz, 2H, phenyl), 7.45 (d, J = 9.0 Hz, 2H, phenyl), 6.98 (s, 2H, phenyl), 3.93 (t, J = 6.6 Hz, 4H, –OCH_2–), 1.81 (m, 4H, –CH_2–), 1.52–1.43 (m, 4H, –CH_2–), 1.30 (m, 48H, –CH_2–), 0.88 (t, J = 7.2 Hz, 6H, –CH_3); $^{13}C\{^1H\}$ NMR (125 MHz, $CDCl_3$, 298 K) δ / ppm = 163.91, 149.09, 145.77, 142.89, 141.73, 137.82, 124.62, 124.35, 98.37, 69.77, 32.11, 29.94, 29.56, 26.23, 22.87, 14.30. Elemental analysis calcd (%) for $C_{52}H_{76}N_2O_4I_2Pt$: C 50.28, H 6.17, N 2.26. Found: C 50.39, H 6.48, N 2.21. MALDI-TOF MS: m/z = 1241.59 $[M]^+$.

PtL6. The procedure was similar to that described for the synthesis of **PtL1**, except Schiff base ligand **L6** (107 mg, 0.12 mmol) was used in place of **L1**. And the residue after solvent evaporation was purified by silica-gel column chromatography with ethyl acetate-methanol (20:1 v/v) as the eluent. Then the product was recrystallized using dichloromethane/hexane to give a red solid. Yield: 80.4 mg (62 %). ^1H NMR (500 MHz, $CDCl_3$, 298 K) δ / ppm = 8.29 (s, 2H, –NCH–), 7.66 (dd, J = 9.0, 1.9 Hz, 2H, phenyl), 7.62 (d, J = 1.9 Hz, 2H, phenyl), 7.11 (s, 2H, phenyl), 7.06 (d, J = 9.0 Hz, 2H, phenyl), 4.02 (t, J = 4.4 Hz, 4H, –OCH_2–), 3.80 (m, 4H, –OCH_2–), 3.74 (m, 4H, –OCH_2–), 3.68 (m, 8H, –OCH_2–), 3.52 (m, 4H, –OCH_2–), 3.27 (s, 6H, –OCH_3); $^{13}C\{^1H\}$ NMR (125 MHz, $CDCl_3$, 298 K) δ / ppm = 163.59, 148.26, 146.66, 142.87, 142.10, 137.82, 124.43, 124.31, 98.81, 71.89, 70.78,69.26, 68.99, 58.86. Elemental analysis calcd (%) for $C_{34}H_{40}N_2O_{10}I_2Pt$: C 37.62, H 3.71, N 2.58. Found: C 37.91, H 3.78, N 2.71. MALDI-TOF MS: m/z = 1085.08 $[M]^+$.

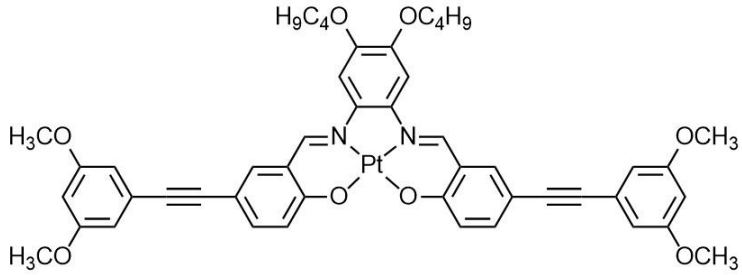

1 (**SBPt-C$_4$-Me**). **PtL1** (181 mg, 0.2 mmol), CuI (3.8 mg, 0.002 mmol), Pd(PPh$_3$)$_4$ (23.1 mg, 0.002 mmol) and 1-ethynyl-3,5-dimethoxybenzene (129.8 mg, 0.8 mmol) were added in dry THF (15 ml) and dry diisopropylamine (45 ml) under nitrogen. The mixture was stirred at 70 ºC for 36 h. The mixture was allowed to cool and filtered. And the residue after solvent evaporation was purified by silica-gel column chromatography with ethyl acetate-methanol (10:1 v/v) as the eluent. Subsequent purification by slow diffusion of hexane into a concentrated dichloromethane solution of **1** afforded a red solid. Yield: 110 mg (56 %). ^{1}H NMR (500 MHz, DMSO-d_6, 298 K) δ / ppm = 9.17 (s, 2H, –NCH–), 8.02 (d, J = 1.7 Hz, 2H, phenyl), 7.69 (s, 2H, phenyl), 7.55 (dd, J = 8.8, 2.2 Hz, 2H, phenyl), 7.00 (d, J = 8.8 Hz, 2H, phenyl), 6.63 (d, J = 2.2 Hz, 4H, phenyl), 6.53 (t, J = 2.2 Hz, 2H, phenyl), 4.05 (t, J = 6.3 Hz, 4H, –OCH$_2$–), 3.78 (s, 12H, –OCH$_3$), 1.78 (m, 4H, –CH$_2$–), 1.50 (m, 4H, –CH$_2$–), 0.99 (t, J = 7.4 Hz, 6H, –CH$_3$); ^{13}C{^{1}H} NMR (125 MHz, DMSO-d_6, 298 K) δ / ppm = 164.21, 160.86, 149.49, 149.13, 139.55, 138.41, 136.79, 124.91, 122.98, 121.86, 109.50, 109.10, 101.58, 99.89, 89.53, 87.96, 68.97, 55.78, 31.35, 19.29, 14.34; Elemental analysis calcd (%) for C$_{48}$H$_{46}$N$_2$O$_8$Pt: C 59.19, H 4.76, N 2.88. Found: C 59.08, H 4.83, N 2.72. MALDI-TOF MS: *m/z* = 973.67 [M]$^+$.

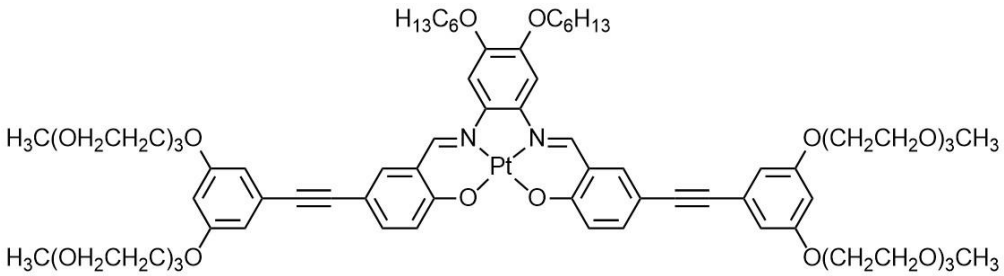

2 (**SBPt-C$_6$-TEG**). **PtL2** (192.3 mg, 0.2 mmol), CuI (3.8 mg, 0.002 mmol), Pd(PPh$_3$)$_4$ (23.1 mg, 0.002 mmol) and 1-ethynyl-3,5-bis(2-(2-(2-methoxyethoxy)ethoxy)ethoxy)benzene (342 mg, 0.8 mmol) were added in dry THF (15 ml) and dry diisopropylamine (45 ml) under the nitrogen. The mixture was stirred at 70 ºC for 36 h. The mixture was allowed to cool and filtered. And the residue after solvent evaporation was purified by silica-gel column chromatography with ethyl

acetate-methanol (10:1 v/v) as the eluent. Subsequent purification by slow diffusion of hexane into a concentrated dichloromethane solution of **2** afforded a red solid. Yield: 141 mg (45 %). ^{1}H NMR (500 MHz, $CDCl_3$, 298 K) δ / ppm = 8.38 (s, 2H, –NCH–), 7.69 (s, 2H, phenyl), 7.54 (s, 2H, phenyl), 7.17 (s, 2H, phenyl), 6.63 (s, 4H, phenyl), 6.48 (s, 2H, phenyl), 4.12 (t, *J* = 4.5 Hz, 8H, –OCH_2–), 4.07 (s, 4H, –OCH_2–), 3.85 (t, *J* = 4.5 Hz, 8H, –OCH_2–), 3.75 (dd, *J* = 6.2, 4.0 Hz, 8H, –OCH_2–), 3.68 (m, 16H, –OCH_2–), 3.56 (dd, *J* = 4.9, 3.2 Hz, 8H, –OCH_2–), 3.38 (s, 12H, –OCH_3), 1.88 (s, 4H, –CH_2–), 1.53 (s, 4H, –CH_2–), 1.39 (m, 8H, –CH_2–), 0.95 (t, *J* = 6.8 Hz, 6H, –CH_3). ^{13}C{^{1}H} NMR (125 MHz, $CDCl_3$, 298 K) δ / ppm = 164.85, 159.78, 149.39, 146.88, 138.48, 138.28, 137.71, 125.01, 122.71, 122.11, 111.28, 110.09, 102.55, 98.95, 88.80, 88.23, 72.08, 70.99, 70.81, 70.71, 69.94, 69.80, 67.71, 59.17, 31.78, 29.32, 25.84, 22.78, 14.22. Elemental analysis calcd (%) for $C_{76}H_{102}N_2O_{20}Pt$: C 58.56, H 6.60, N 1.80. Found: C 58.73, H 6.35, N 1.72. MALDI-TOF MS: *m/z* = 1557.52 $[M]^+$.

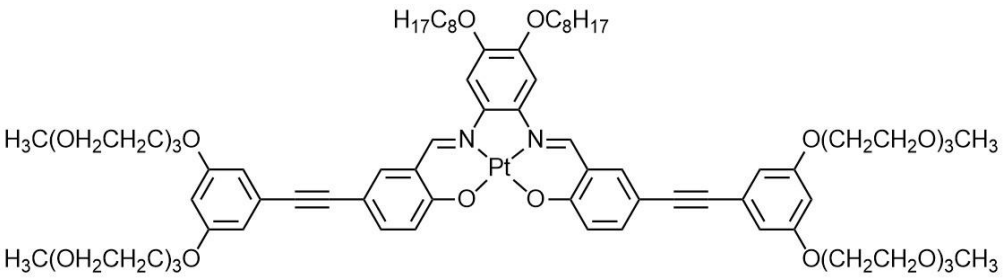

3 (**SBPt-C_8-TEG**). The procedure was similar to that described for the synthesis of complex **2**, except **PtL3** (203 mg, 0.2 mmol) was used in place of **PtL2**. Subsequent purification by slow diffusion of hexane into a concentrated dichloromethane solution of **3** afforded a red solid. Yield: 136 mg (42 %). ^{1}H NMR (500 MHz, $CDCl_3$, 298 K) δ / ppm = 8.43 (s, 2H, –NCH–), 7.73 (s, 2H, phenyl), 7.58 (d, *J* = 8.9 Hz, 2H, phenyl), 7.31 (d, *J* = 8.9 Hz, 2H, phenyl), 7.21 (s, 2H, phenyl), 6.66 (s, 4H, phenyl), 6.50 (s, 2H, phenyl), 4.14 (t, *J* = 5.5 Hz, 8H, –OCH_2–), 4.10 (t, *J* = 5.5 Hz, 4H, –OCH_2–), 3.89 (m, 8H, –OCH_2–), 3.77 (m, 8H, –OCH_2–), 3.70 (m, 16H, –OCH_2–), 3.58 (m, 8H, –OCH_2–), 3.40 (d, *J* = 7.4 Hz, 12H, –OCH_3), 1.91 (m, 4H, –CH_2–), 1.52 (m, 4H, –CH_2–), 1.38 (m, 16H, –CH_2–), 0.93 (t, *J* = 6.7 Hz, 6H, –CH_3); ^{13}C{^{1}H} NMR (125 MHz, $CDCl_3$, 298 K) δ / ppm = 164.85, 159.77, 149.39, 146.88, 138.51, 138.27, 137.70, 125.00, 122.70, 122.12, 111.26, 110.08, 102.53, 98.99, 88.79, 88.23, 72.07, 70.99, 70.80, 70.72, 69.96, 69.79, 67.70, 59.17, 32.00, 29.60, 29.39, 26.18, 22.84, 14.28. Elemental analysis calcd (%) for $C_{80}H_{110}N_2O_{20}Pt$: C 59.50, H 6.87, N 1.73. Found: C 59.70, H 6.89, N 1.58. MALDI-TOF MS: *m/z* = 1613.64 $[M]^+$.

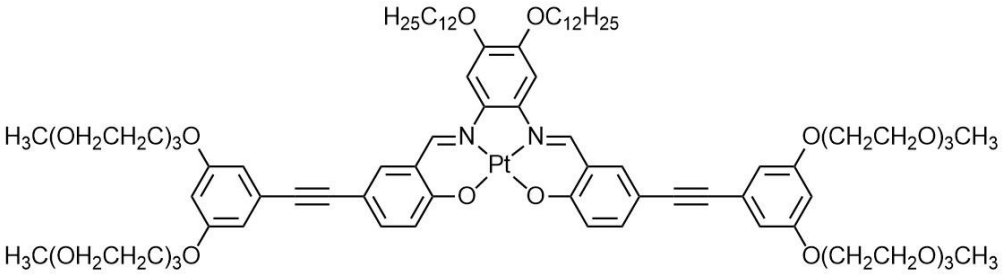

4 (**SBPt-C$_{12}$-TEG**). The procedure was similar to that described for the synthesis of complex **2**, except **PtL4** (226 mg, 0.2 mmol) was used in place of **PtL2**. Subsequent purification by slow diffusion of hexane into a concentrated dichloromethane solution of **4** afforded a red solid. Yield: 139 mg (40 %).^{1}H NMR (500 MHz, $CDCl_3$, 298 K) δ / ppm = 8.42 (s, 2H, –NCH–), 7.72 (s, 2H, phenyl), 7.57 (d, J = 8.9 Hz, 2H, phenyl), 7.31 (d, J = 8.9 Hz, 2H, phenyl), 7.21 (s, 2H, phenyl), 6.65 (s, 4H, phenyl), 6.50 (s, 2H, phenyl), 4.15 (t, J = 5.6 Hz , 8H, –OCH_2–), 4.05 (t, J = 5.6 Hz, 4H, –OCH_2–), 3.87 (t, J = 9.8 Hz, 8H, –OCH_2–), 3.78 (m, 8H, –OCH_2–), 3.69 (m, 16H, –OCH_2–), 3.57 (m, 8H, –OCH_2–), 3.40 (s, 12H, –OCH_3), 1.91 (m, 4H, –CH_2–), 1.55 (m, 4H, –CH_2–), 1.44 (s, 4H, –CH_2–), 1.30 (s, 28H, –CH_2–), 0.90 (t, J = 6.6 Hz, 6H, –CH_3); ^{13}C{^{1}H} NMR (125 MHz, $CDCl_3$, 298 K) δ / ppm = 165.05, 159.80, 149.55, 147.00, 138.65, 138.15, 137.77, 124.99, 122.88, 122.12, 111.30, 110.13, 102.62, 99.06, 88.75, 88.24, 72.09, 71.01, 70.75, 69.81, 67.73, 59.19, 32.08, 29.84, 29.52, 26.24, 22.84, 14.27. Elemental analysis calcd (%) for $C_{88}H_{126}N_2O_{20}Pt$: C 61.20, H 7.35, N 1.62. Found: C 60.87, H 7.61, N 1.53. MALDI-TOF MS: m/z = 1725.59 $[M]^+$.

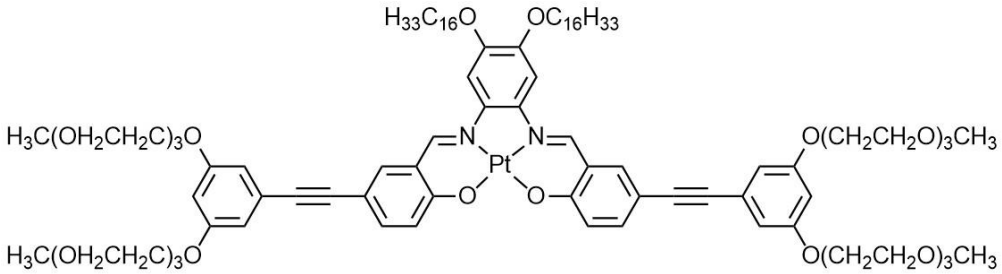

5 (**SBPt-C$_{16}$-TEG**). The procedure was similar to that described for the synthesis of complex **2**, except **PtL5** (248 mg 0.2 mmol) was used in place of **PtL2**. Subsequent purification by slow diffusion of hexane into a concentrated dichloromethane solution of **5** afforded a red solid. Yield: 145 mg (39 %).^{1}H NMR (500 MHz, $CDCl_3$, 298 K) δ / ppm = 8.38 (s, 2H, –NCH–), 7.69 (s, 2H, phenyl), 7.55 (d, J = 8.9 Hz, 2H, phenyl), 7.29 (d, J = 8.9 Hz, 2H, phenyl), 7.19 (s, 2H, phenyl), 6.64 (s, 4H, phenyl), 6.50 (s, 2H, phenyl), 4.10 (t, J = 5.5 Hz, 8H, –OCH_2–) 4.08 (t, J = 5.5 Hz, 4H, –OCH_2–), 3.85 (t, J = 4.9 Hz, 8H, –OCH_2–), 3.77 (m, 8H, –OCH_2–), 3.72 (m, 8H, –OCH_2–), 3.69

(m, 8H, –OCH_2–), 3.58 (m, 8H, –OCH_2–), 3.40 (s, 12H, –OCH_3), 1.91 (m, 4H, –CH_2–), 1.55 (m, 4H, –CH_2–), 1.42 (m, 4H, –CH_2–), 1.30 (m, 44H, –CH_2–), 0.90 (t, J = 7.1 Hz, 6H, –CH_3); $^{13}C\{^1H\}$ NMR (125 MHz, $CDCl_3$, 298 K) δ / ppm = 165.02, 159.79, 149.53, 146.97, 138.28, 137.75, 124.99, 124.84, 122.12, 111.28, 110.11, 102.60, 99.05, 88.75, 88.24, 72.08, 71.01, 70.83, 69.81, 67.72, 59.18, 31.92, 29.90, 29.52, 26.24, 22.84, 14.27. Elemental analysis calcd (%) for $C_{96}H_{142}N_2O_{20}Pt$: C 62.69, H 7.78, N 1.52. Found: C 62.53, H 7.91, N 1.46. MALDI-TOF MS: m/z = 1837.64 $[M]^+$.

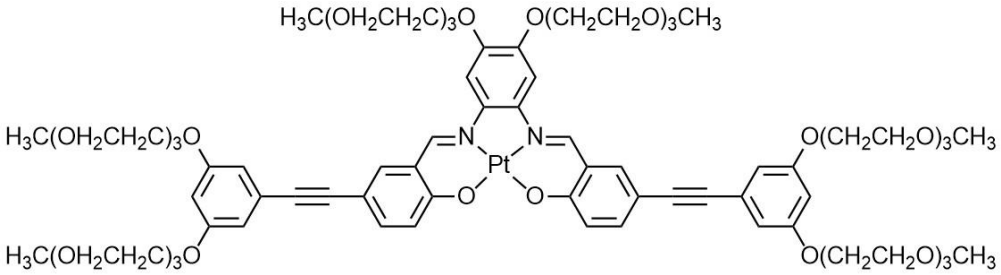

6 (**SBPt-TEG-TEG**). The procedure was similar to that described for the synthesis of complex **2**, except **PtL6** (217 mg, 0.2 mmol) was used in place of **PtL2**. Subsequent purification by slow diffusion of hexane into a concentrated dichloromethane solution of **6** afforded a red oil. Yield: 140 mg (42 %). ^1H NMR (500 MHz, $CDCl_3$, 298 K) δ / ppm = 8.54 (s, 2H, –NCH–), 7.73 (s, 2H, phenyl), 7.61 (d, J = 8.9 Hz, 2H, phenyl), 7.42 (s, 2H, phenyl), 7.33 (d, J = 8.9 Hz, 2H, phenyl), 6.67 (s, 4H, phenyl), 6.52 (s, 2H, phenyl), 4.26 (s, 4H, –OCH_2–), 4.15 (t, J = 4.9 Hz, 8H, –OCH_2–), 3.88 (m, 12H, –OCH_2–), 3.79 (m, 12H, –OCH_2–), 3.69 (m, 24H, –OCH_2–), 3.58 (m, 8H, –OCH_2–), 3.51(m, 4H, –OCH_2–), 3.41 (s, 12H, –OCH_2–), 3.30 (s, 6H, –OCH_3); $^{13}C\{^1H\}$ NMR (125 MHz, $CDCl_3$, 298 K) δ / ppm = 164.80, 159.82, 148.88, 147.63, 138.49, 137.87, 125.09, 122.37, 122.18, 111.41, 110.17, 102.61, 99.68, 88.86, 88.19, 72.08, 72.01, 71.08, 70.99, 70.82, 70.73, 69.80, 69.67, 69.39, 67.74, 59.18, 58.98. Elemental analysis calcd (%) for $C_{78}H_{106}N_2O_{26}Pt$: C 55.67, H 6.35, N 1.66. Found: C 55.38, H 6.74, N 1.49. MALDI-TOF MS: m/z = 1681.94 $[M]^+$.

NMR Spectra

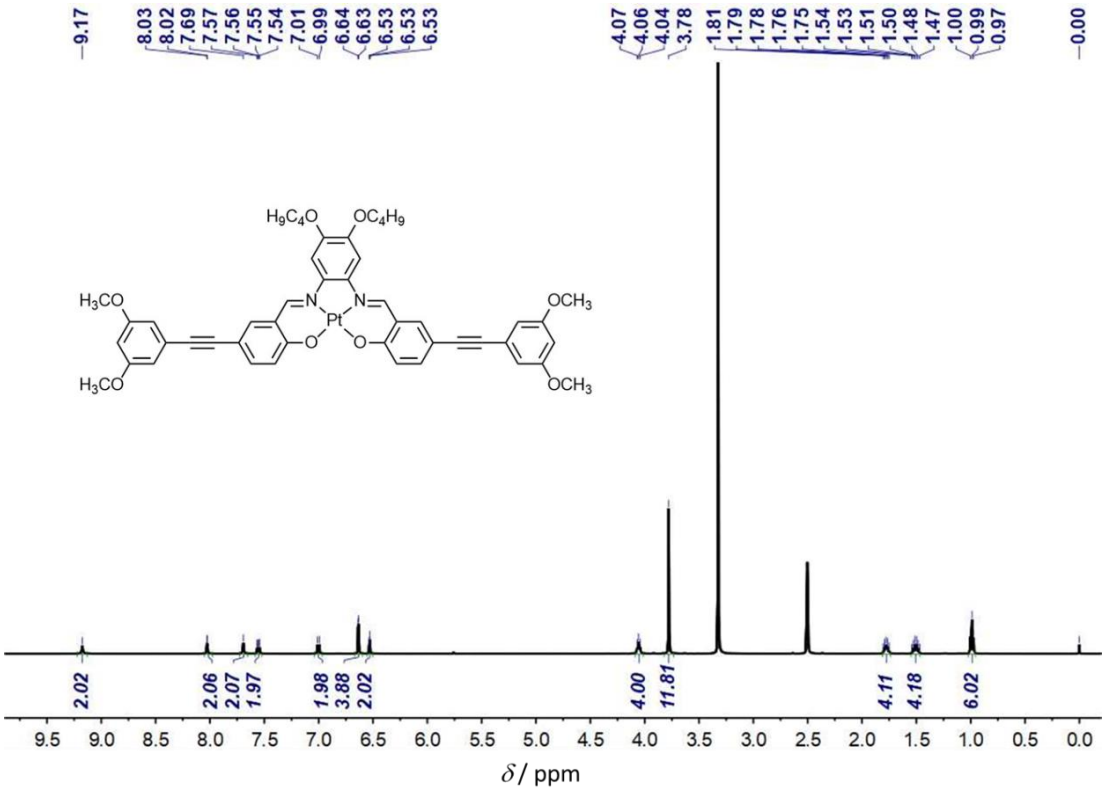

Figure S1. ^{1}H NMR spectrum of **1** in DMSO-d_6 at 298 K.

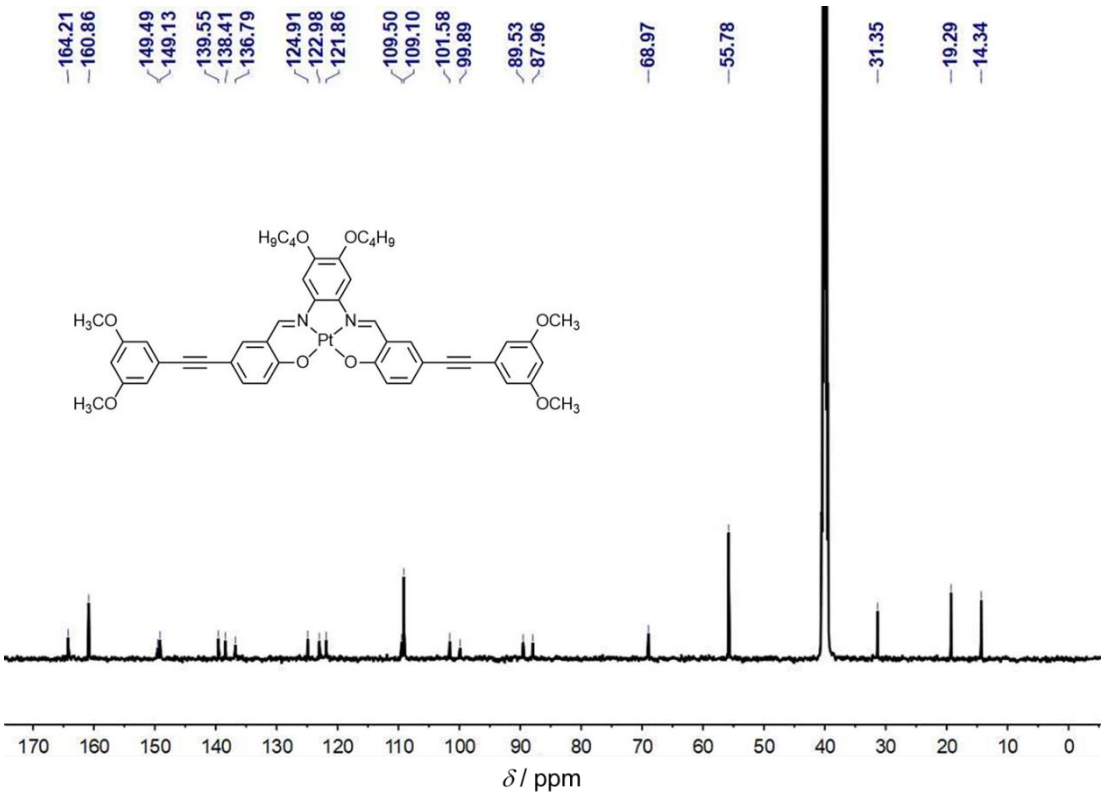

Figure S2. ^{13}C{^{1}H} NMR spectrum of **1** in DMSO-d_6 at 298 K.

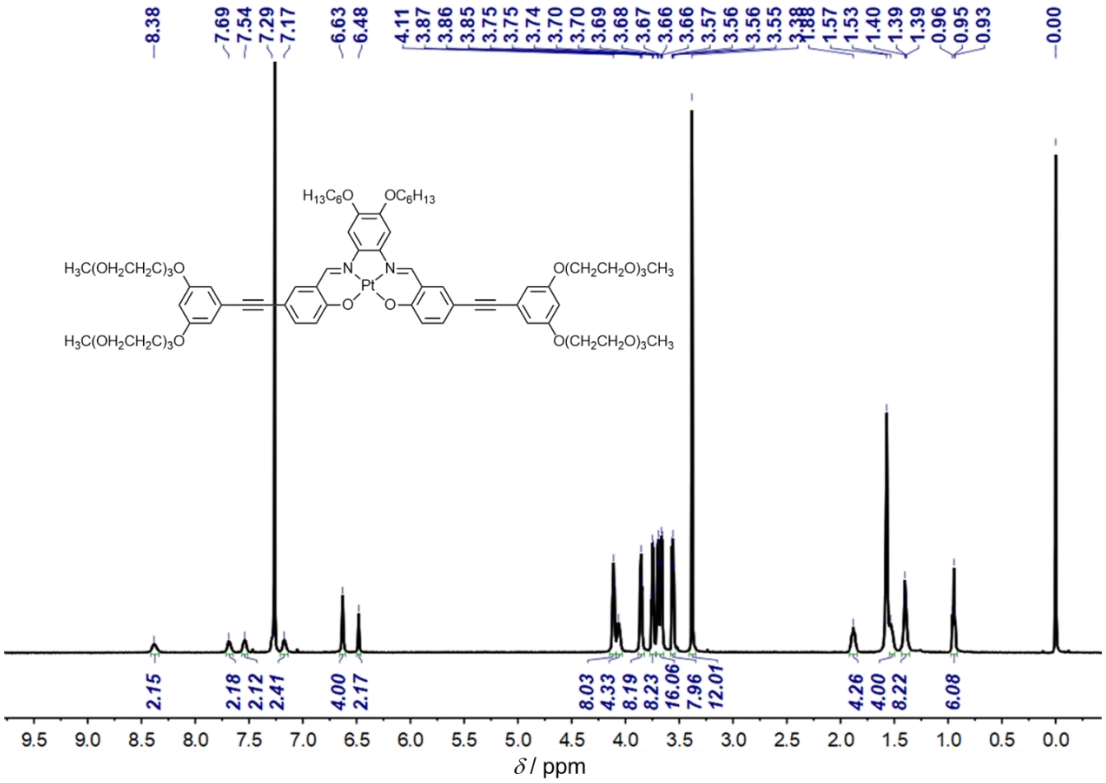

Figure S3. ^{1}H NMR spectrum of **2** in $CDCl_3$ at 298 K.

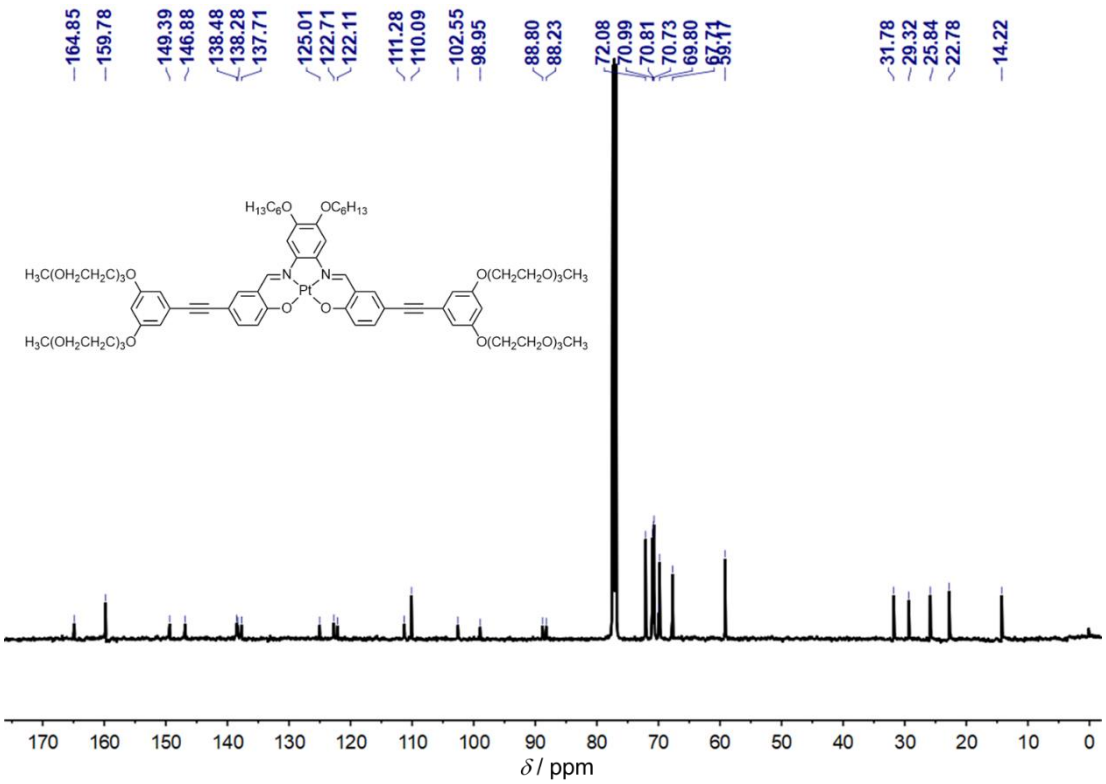

Figure S4. ^{13}C{^{1}H} NMR spectrum of **2** in $CDCl_3$ at 298 K.

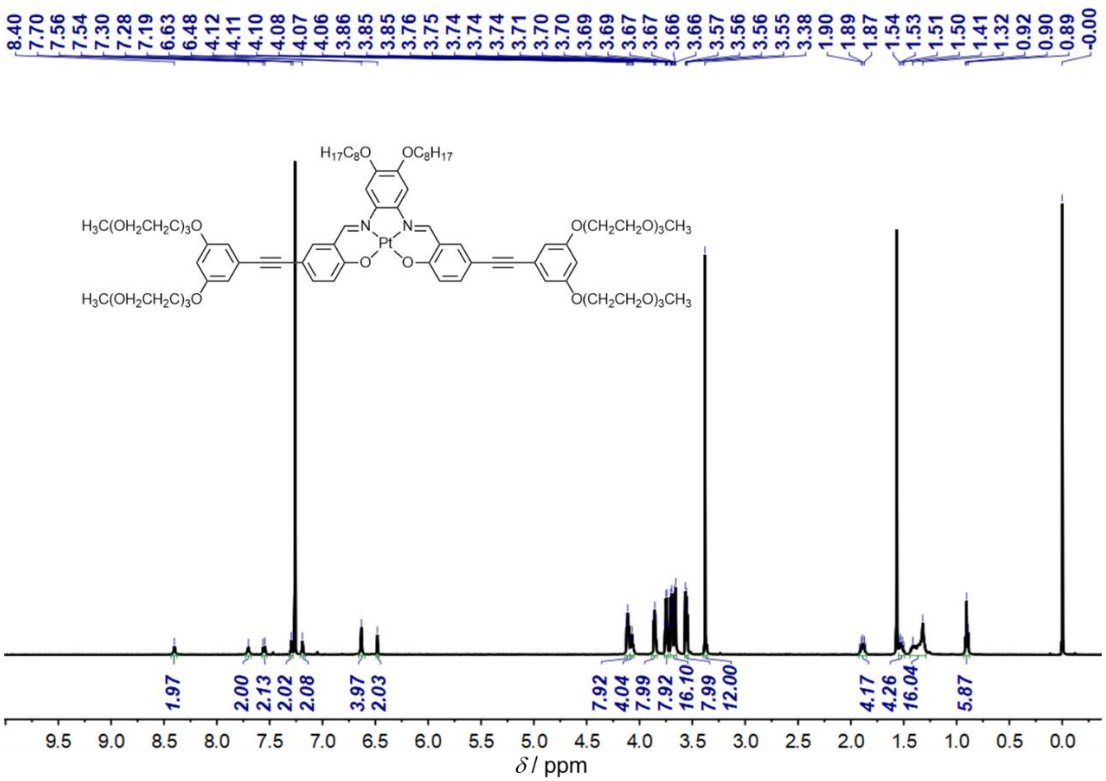

Figure S5. ^{1}H NMR spectrum of **3** in $CDCl_3$ at 298 K.

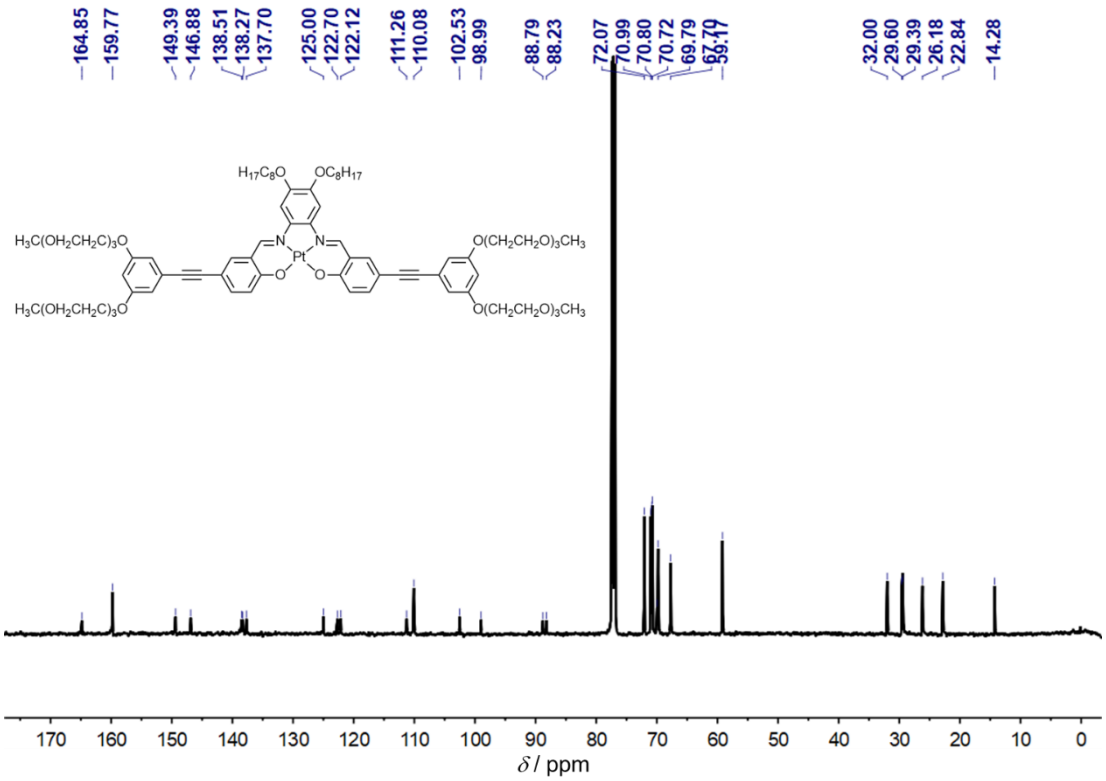

Figure S6. ^{13}C{^{1}H} NMR spectrum of **3** in $CDCl_3$ at 298 K.

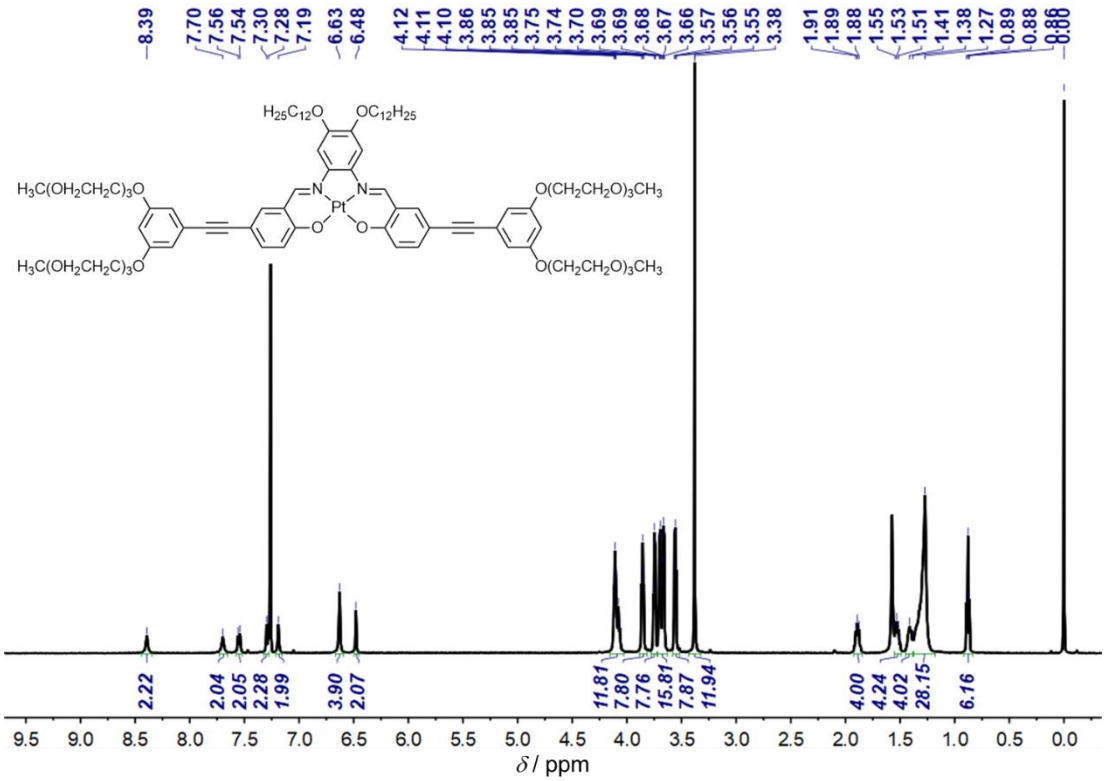

Figure S7. ^{1}H NMR spectrum of **4** in $CDCl_3$ at 298 K.

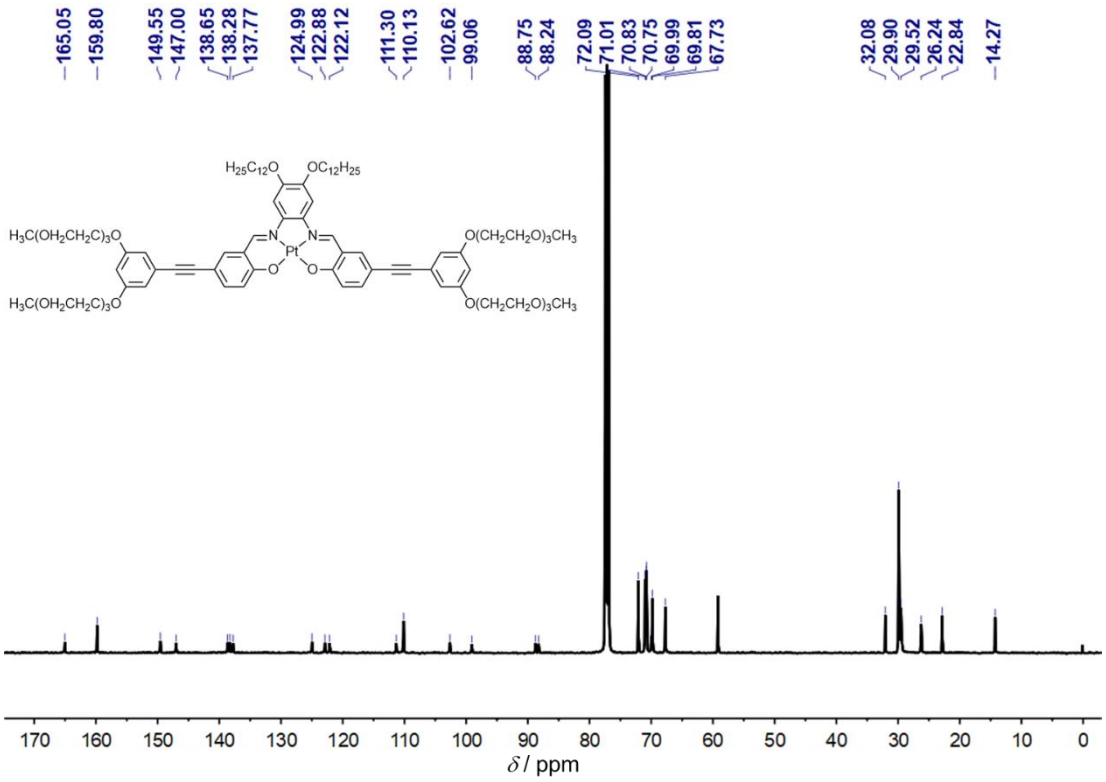

Figure S8. ^{13}C{^{1}H} NMR spectrum of **4** in $CDCl_3$ at 298 K.

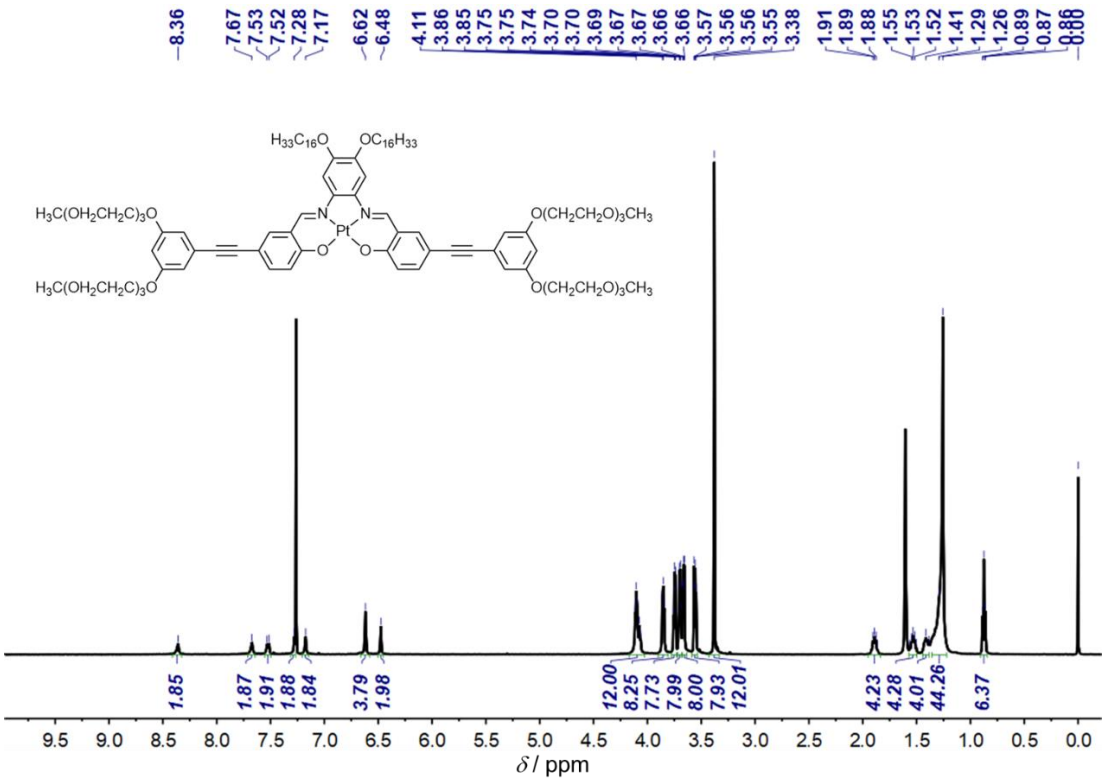

Figure S9. ^{1}H NMR spectrum of **5** in $CDCl_3$ at 298 K.

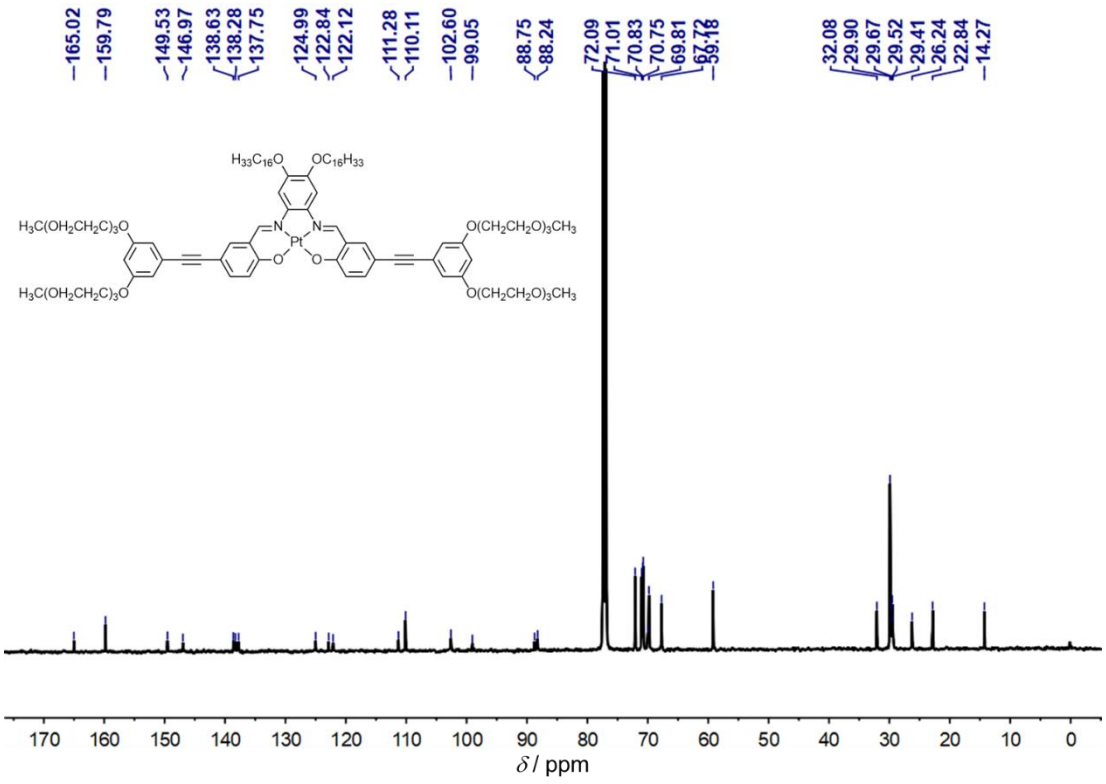

Figure S10. $^{13}C\{^{1}H\}$ NMR spectrum of **5** in $CDCl_3$ at 298 K.

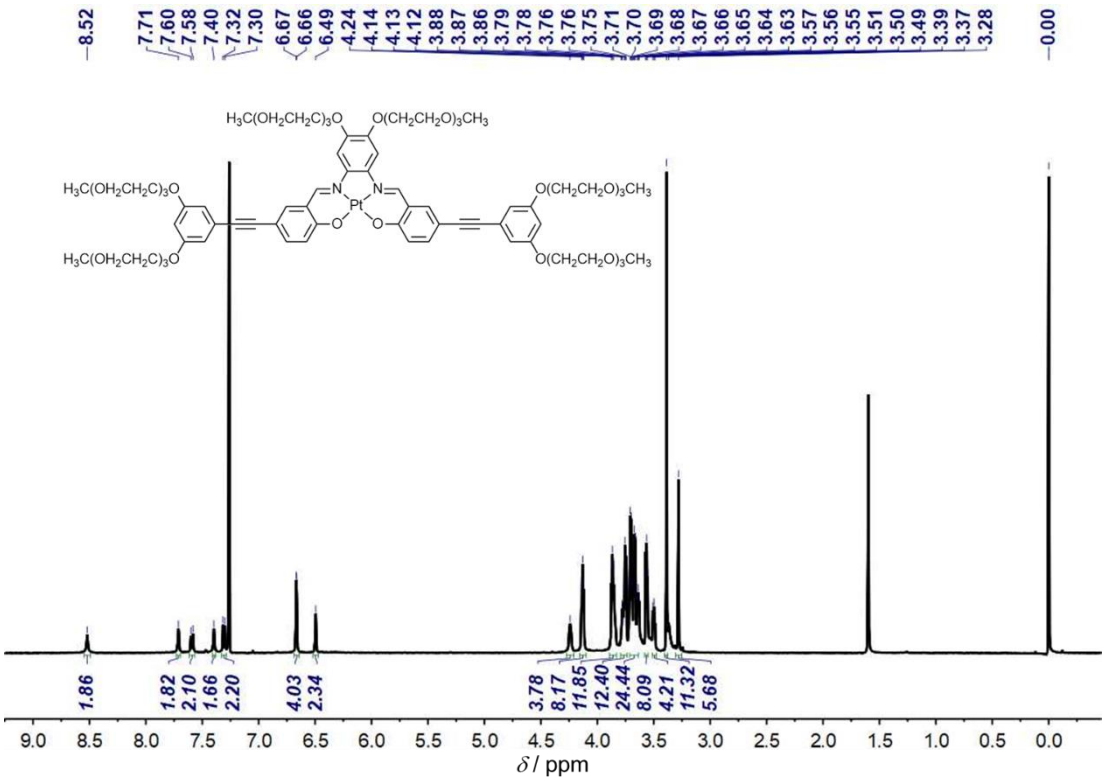

Figure S11. ^{1}H NMR spectrum of **6** in $CDCl_3$ at 298 K.

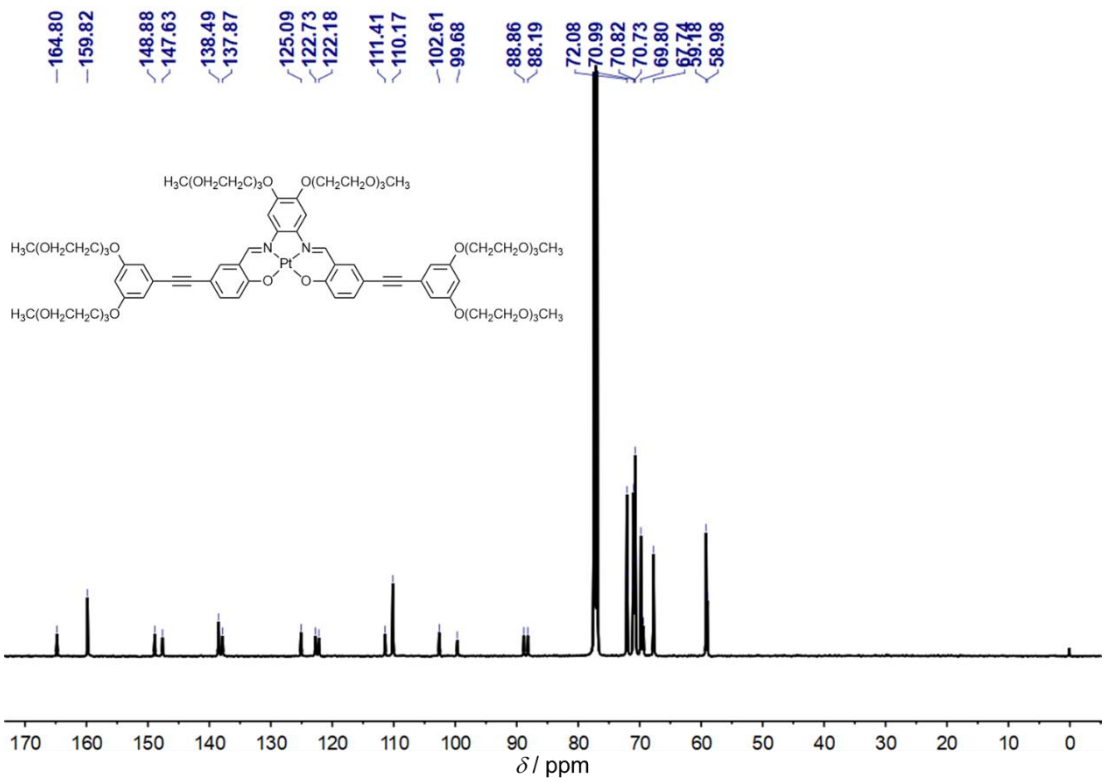

Figure S12. ^{13}C{^{1}H} NMR spectrum of **6** in $CDCl_3$ at 298 K.

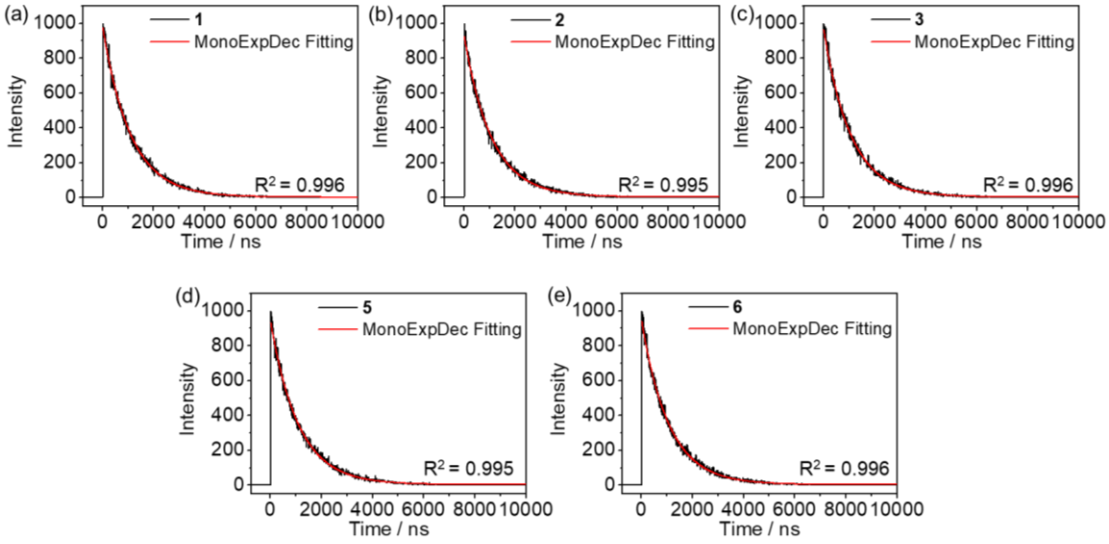

Figure S13. Phosphorescence decay traces (detected at the emission band maxima) of (a) **1**, (b) **2**, (c) **3**, (d) **5** and (e) **6** in degassed DMSO solutions at 298 K showing monoexponential decay.

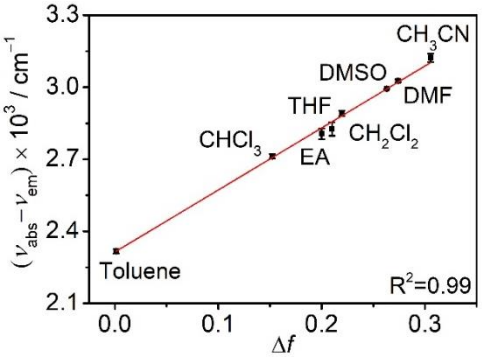

Figure S14. The Lippert–Mataga absorption coefficient plot of the complex **2** on orientation polarization (Δf) versus the solvent change under degassed conditions in the concentration regime of 10^{-5} M at 298 K.

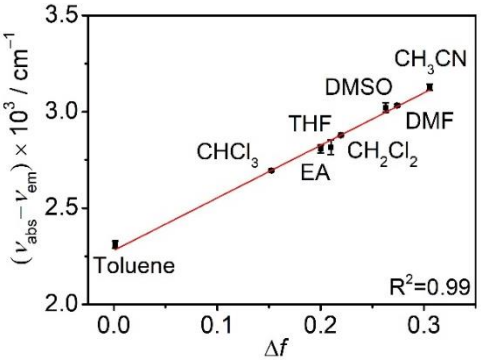

Figure S15. The Lippert–Mataga absorption coefficient plot of the complex **3** on orientation polarization (Δf) versus the solvent change under degassed conditions in the concentration regime of 10^{-5} M at 298 K.

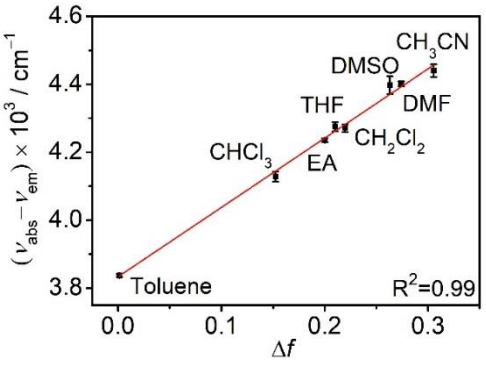

Figure S16. The Lippert–Mataga absorption coefficient plot of the complex **4** on orientation polarization (Δ*f*) versus the solvent change under degassed conditions in the concentration regime of 10^{-5} M at 298 K.

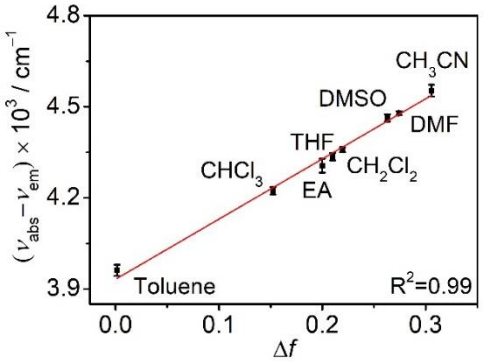

Figure S17. The Lippert–Mataga absorption coefficient plot of the complex **5** on orientation polarization (Δ*f*) versus the solvent change under degassed conditions in the concentration regime of 10^{-5} M at 298 K.

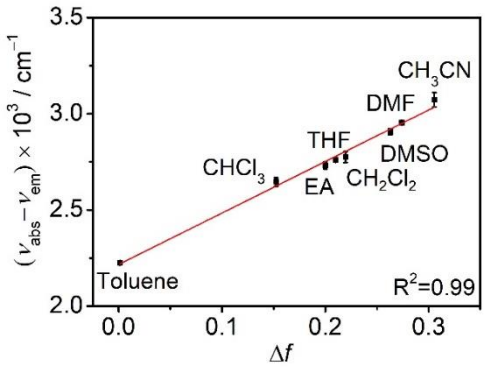

Figure S18. The Lippert–Mataga absorption coefficient plot of the complex **6** on orientation polarization (Δ*f*) versus the solvent change under degassed conditions in the concentration regime of 10^{-5} M at 298 K.

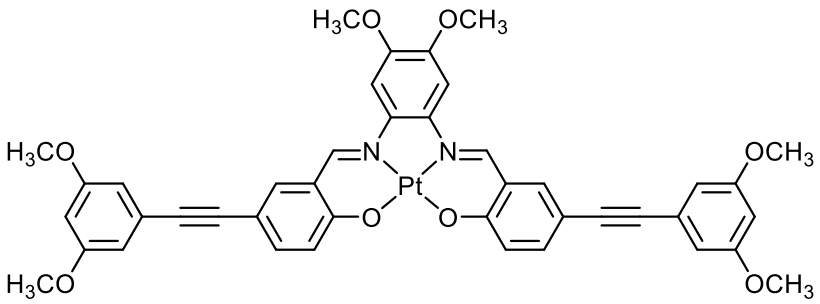

Figure S19. Structure of complex **7**, is used as a model complex for computational study to elucidate the behavior of complexes **1**–**6**.

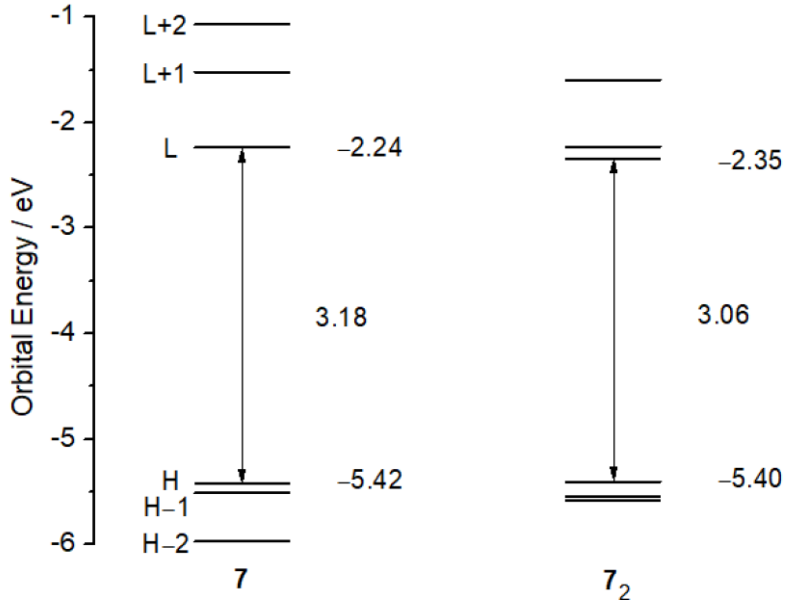

Figure S20. Orbital energy diagram of **7** and the dimer $\mathbf{7}_2$, with H=HOMO and L=LUMO.

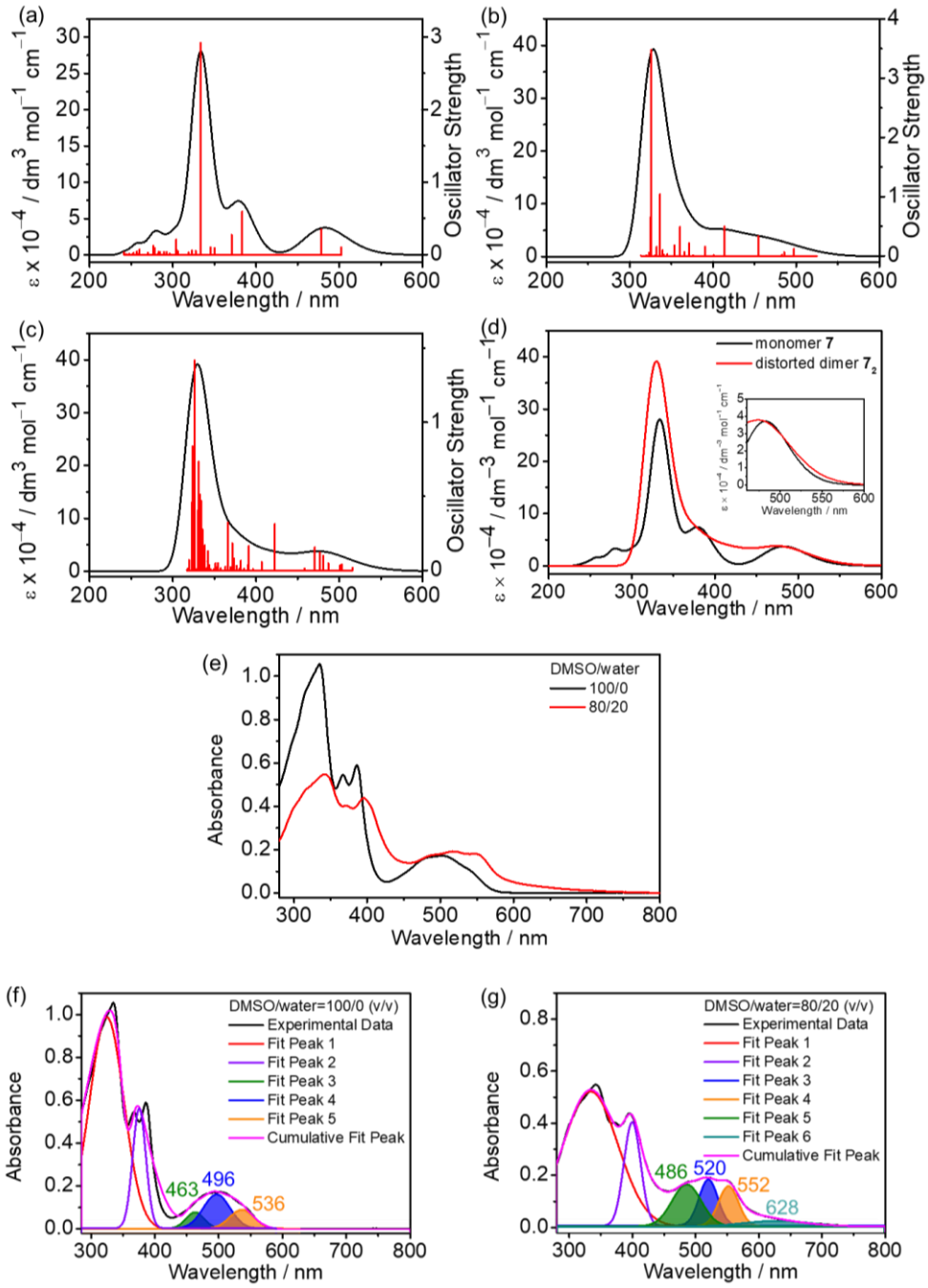

Figure S21. Simulated absorption spectra of the (a) monomer **7**, (b) dimer $\mathbf{7}_2$, (c) distorted dimer $\mathbf{7}_2$ (slightly tilting the plane of one monomer with respect to the other). The heights of the vertical straight lines are the calculated oscillator strengths of the corresponding vertical transitions. (d) Overlaid simulated absorption spectra of the monomer **7** and distorted dimer $\mathbf{7}_2$. (Inset) The expanded simulated absorption spectra in the range of 460–600 nm. (e) UV–Vis absorption spectra of **4** in pure DMSO and 20 % water–DMSO (v/v) solutions in the concentration regime of 10^{-5} M. UV–Vis absorption spectra of **4** in (f) pure DMSO and (g) 20 % water–DMSO (v/v) and their corresponding fitted spectra showing the deconvoluted UV–vis absorption bands with their

absorption maxima.

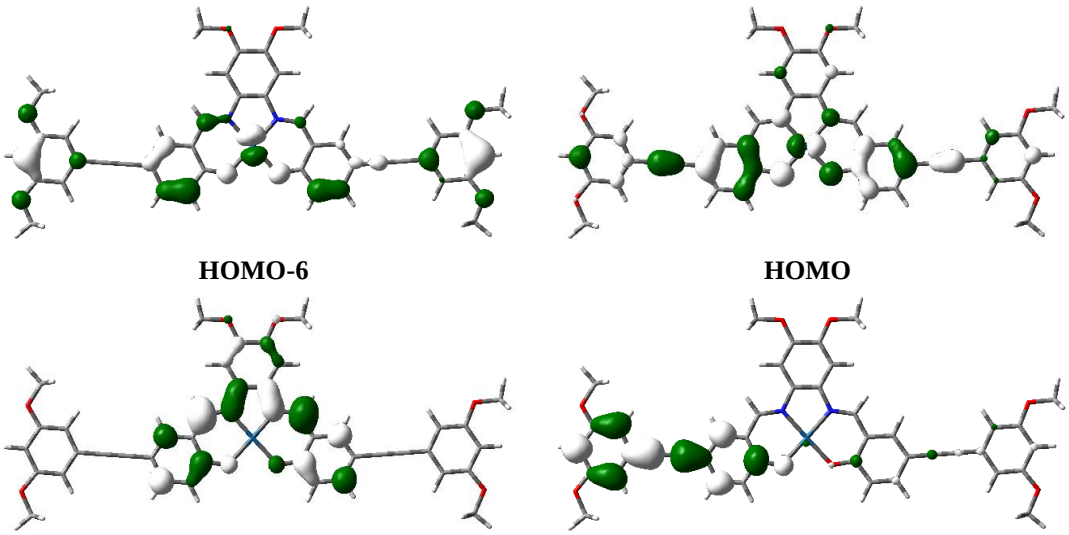

Figure S22. Spatial plots (isovalue = 0.03) of the selected molecular orbitals of **7** at the ground–state (S_0) geometry.

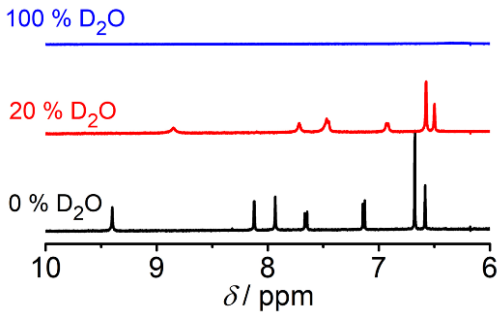

Figure S23. Partial ^{1}H NMR spectra of complex **6** in the DMSO-d_6, 20 % D_2O in DMSO-d_6 and 100 % D_2O ([Pt] = 2.0×10^{-4} M) at 298 K.

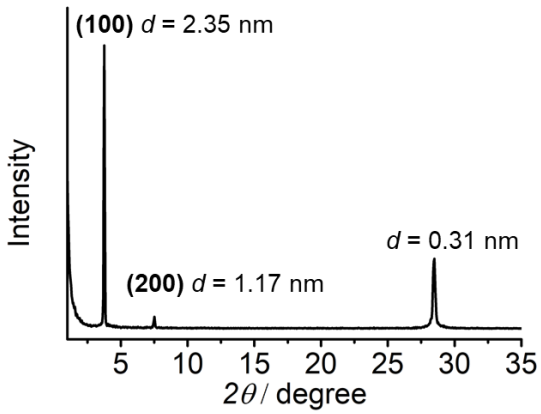

Figure S24. X-Ray diffraction (XRD) pattern of a thin film of prepared from **6** in water at 298 K.

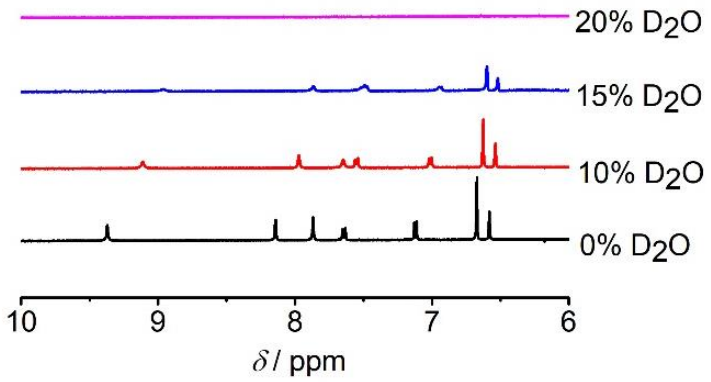

Figure S25. Partial ^{1}H NMR spectral traces of **2** upon increasing D_2O content in DMSO-d_6 from 0 to 20 % at 298 K ([Pt] = ~10^{-4} M).

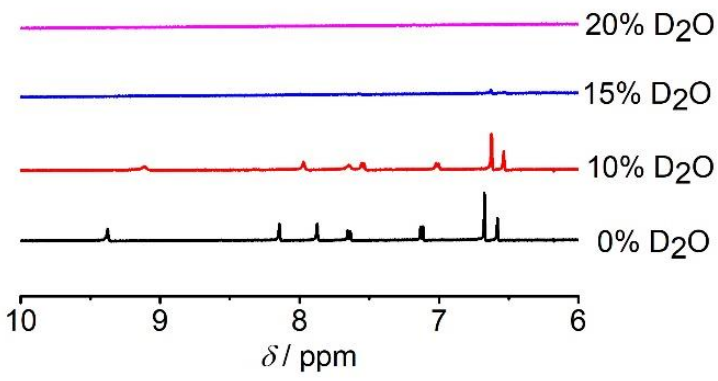

Figure S26. Partial ^{1}H NMR spectral traces of **3** upon increasing D_2O content in DMSO-d_6 from 0 to 20 % at 298 K ([Pt] = ~10^{-4} M).

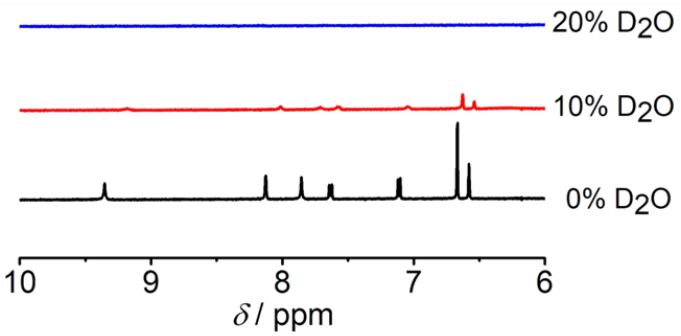

Figure S27. Partial ^{1}H NMR spectral traces of **4** upon increasing D_2O content in DMSO-d_6 from 0 to 20 % at 298 K ([Pt] = ~10^{-4} M).

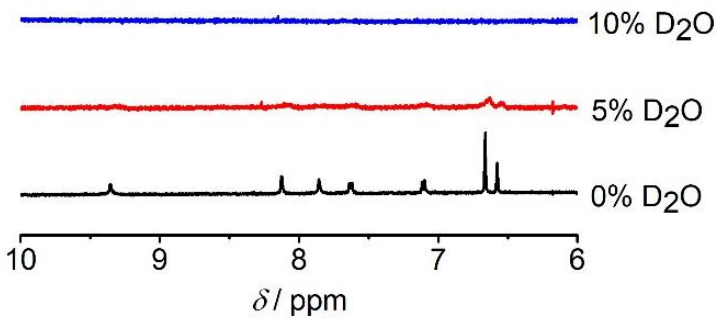

Figure S28. Partial ^{1}H NMR spectral traces of **5** upon increasing D_2O content in DMSO-d_6 from 0 to 10 % at 298 K ([Pt] = ~10^{-4} M).

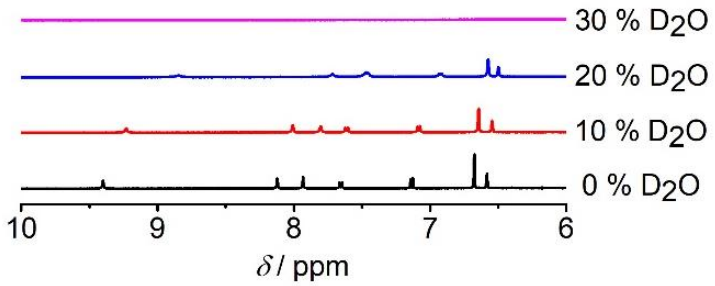

Figure S29. Partial ^{1}H NMR spectral traces of **6** upon increasing D_2O content in DMSO-d_6 from 0 to 30 % at 298 K ([Pt] = ~10^{-4} M).

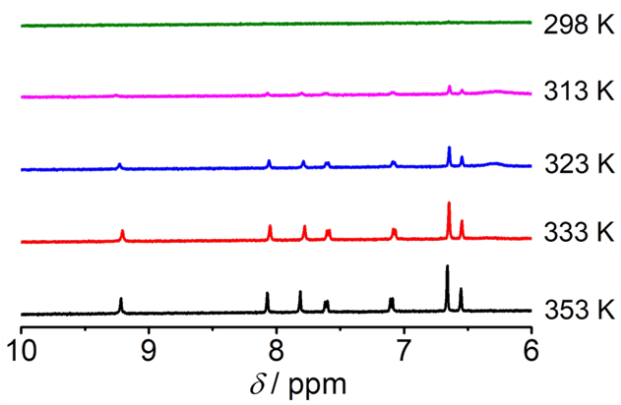

Figure S30. Partial ^{1}H NMR spectral traces of **4** with 20 % D_2O content in DMSO-d_6 with increasing temperature from 298 to 353 K ([Pt] = ~10^{-4} M).

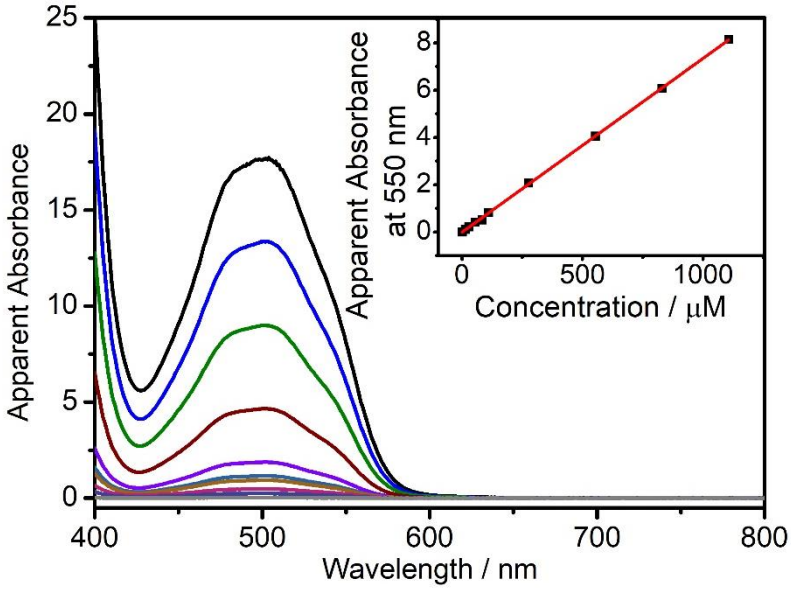

Figure S31. Electronic absorption spectra of **2** in DMSO solutions at various concentrations (1.383 to 1106 μM). Inset: Plot of absorbance at 550 nm against concentration. The apparent absorbance values have been obtained by correcting to a 1-cm path length equivalence.

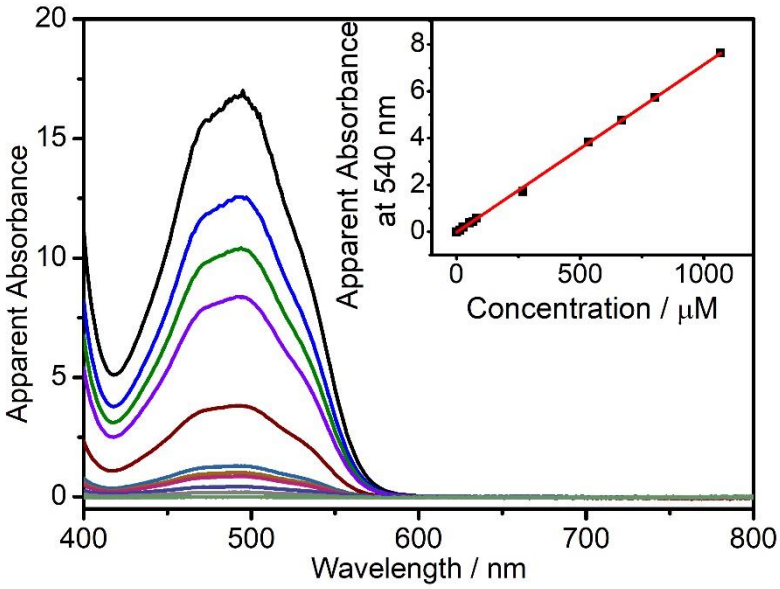

Figure S32. Electronic absorption spectra of **3** in DMSO solutions at various concentrations (1.335 to 1068 μM). Inset: Plot of absorbance at 540 nm against concentration. The apparent absorbance values have been obtained by correcting to a 1-cm path length equivalence.

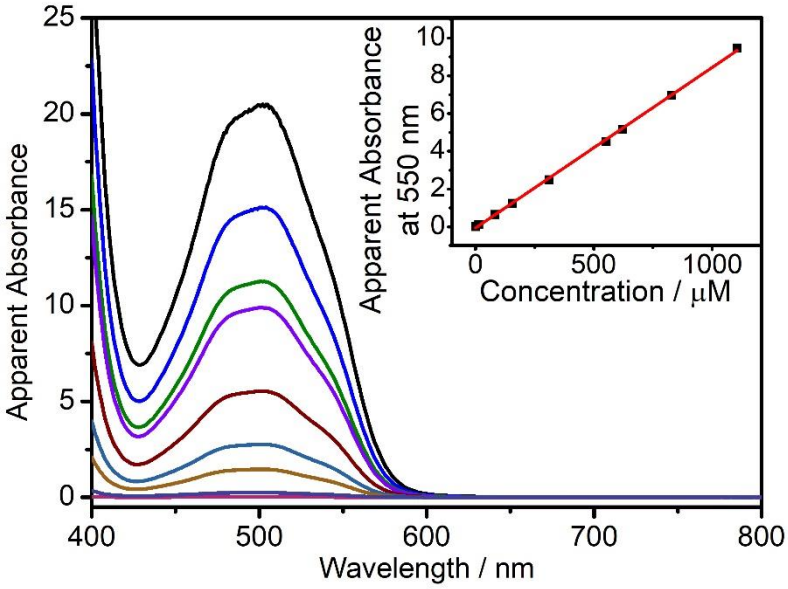

Figure S33. Electronic absorption spectra of **4** in DMSO solutions at various concentrations (1.383 to 1106 μM). Inset: Plot of absorbance at 550 nm against concentration. The apparent absorbance values have been obtained by correcting to a 1-cm path length equivalence.

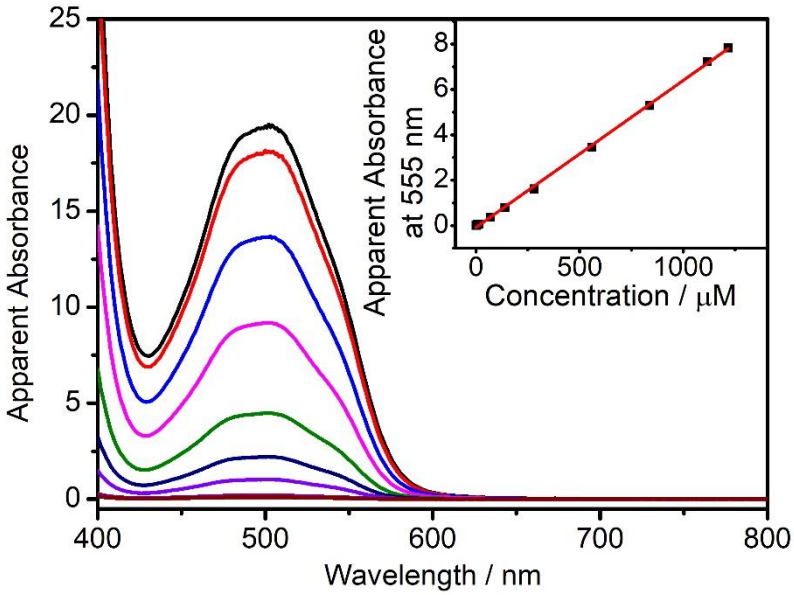

Figure S34. Electronic absorption spectra of **5** in DMSO solutions at various concentrations (6.98 to 1215 μM). Inset: Plot of absorbance at 555 nm against concentration. The apparent absorbance values have been obtained by correcting to a 1-cm path length equivalence.

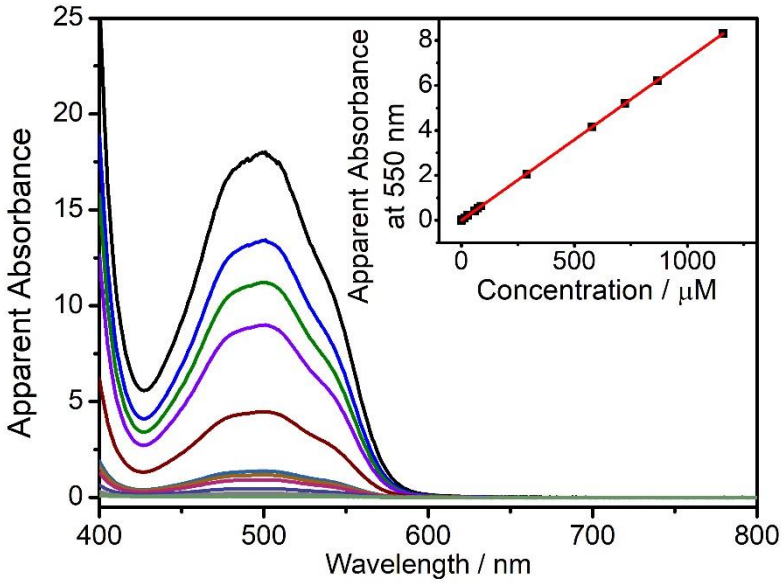

Figure S35. Electronic absorption spectra of **6** in DMSO solutions at various concentrations (1.448 to 1158 μM). Inset: Plot of absorbance at 550 nm against concentration. The apparent absorbance values have been obtained by correcting to a 1-cm path length equivalence.

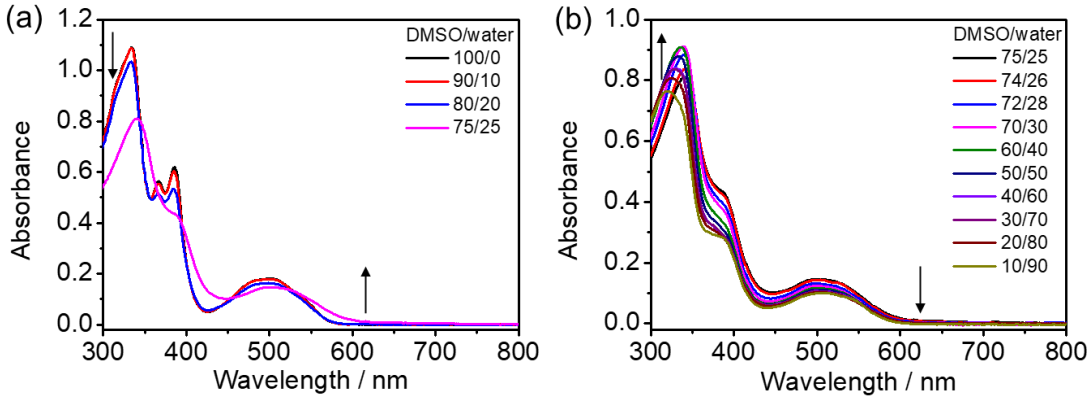

Figure S36. UV–Vis absorption spectral changes of **2** in DMSO solutions upon increasing water content from (a) 0 to 25 % and (b) 25 to 90 % in the concentration regime of 10^{-5} M.

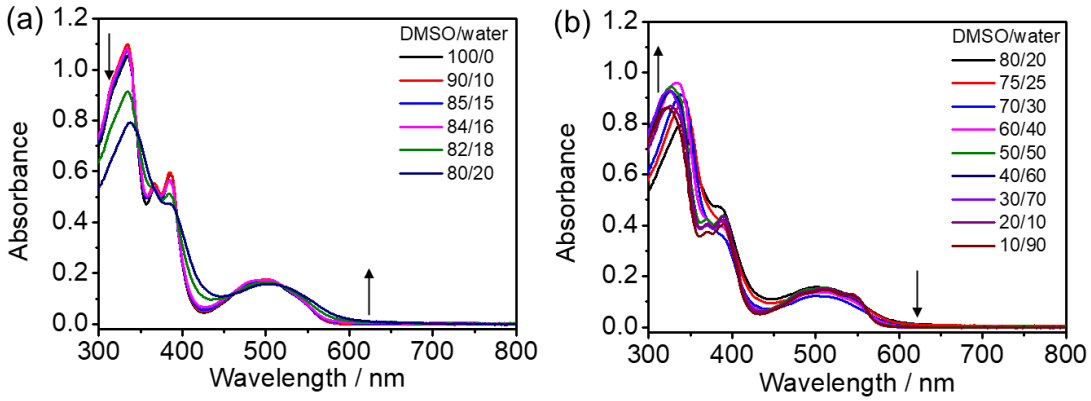

Figure S37. UV–Vis absorption spectral changes of **3** in DMSO solutions upon increasing water content from (a) 0 to 20 % and (b) 20 to 90 % in the concentration regime of 10^{-5} M.

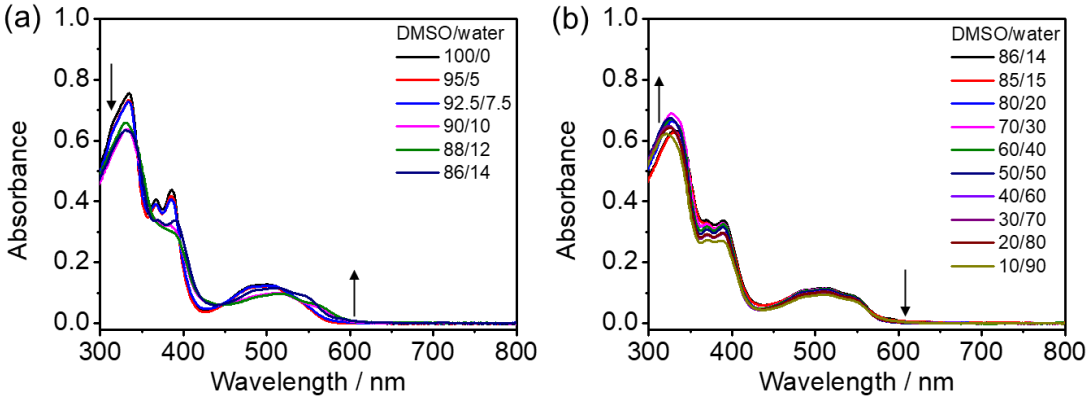

Figure S38. UV–Vis absorption spectral changes of **5** in DMSO solutions upon increasing water content from (a) 0 to 14 % and (b) 14 to 90 % in the concentration regime of 10^{-5} M.

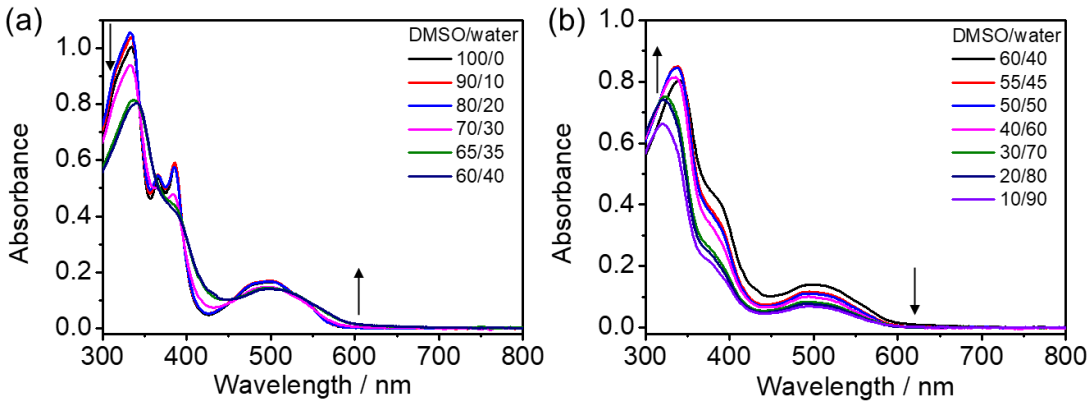

Figure S39. UV–Vis absorption spectral changes of **6** in DMSO solutions upon increasing water content from (a) 0 to 40 % and (b) 40 to 90 % in the concentration regime of 10^{-5} M.

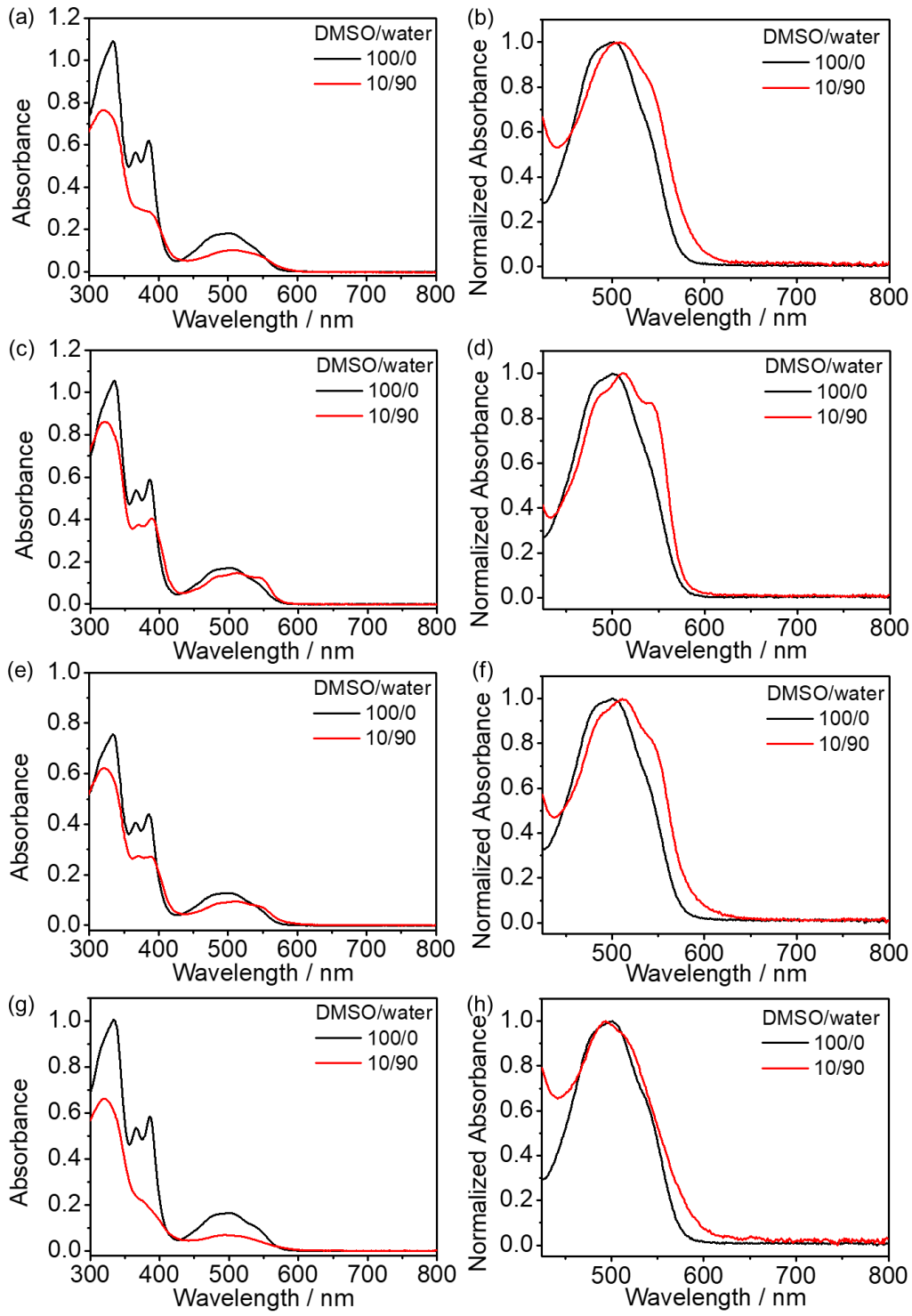

Figure S40. UV–Vis absorption spectral changes of (a) **2**, (c) **3**, (e) **5** and (g) **6** and normalized UV–vis absorption spectra of (b) **2**, (d) **3**, (f) **5** and (h) **6** in DMSO solutions and in 90 % water–DMSO (v/v) solutions in the concentration regime of 10^{-5} M.

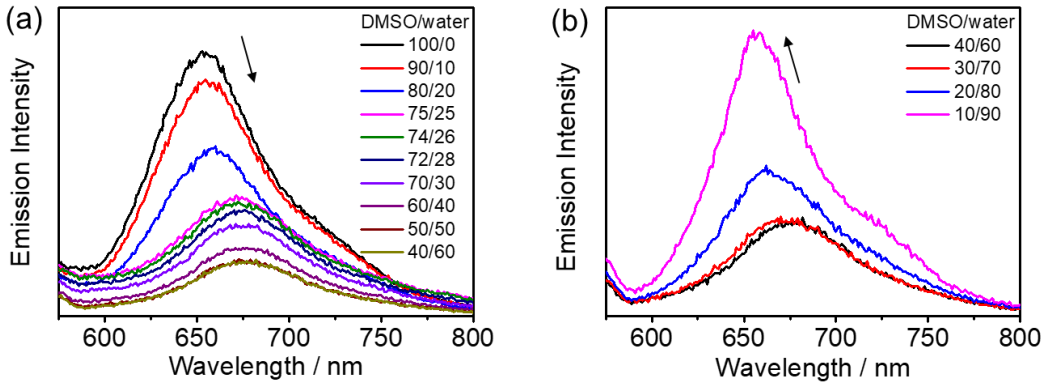

Figure S41. Emission spectral changes of **2** in DMSO solutions upon increasing water content from (a) 0 to 60 % and (b) 60 to 90 % in the concentration regime of 10^{-5} M.

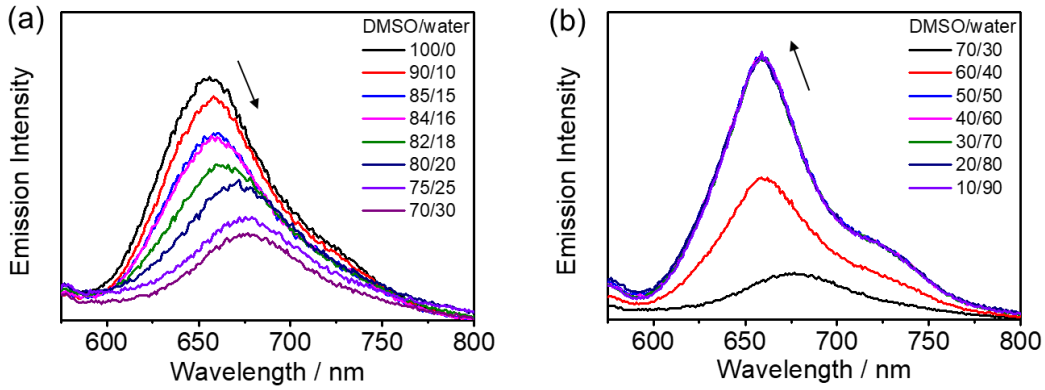

Figure S42. Emission spectral changes of **3** in DMSO solutions upon increasing water content from (a) 0 to 30 % and (b) 30 to 90 % in the concentration regime of 10^{-5} M.

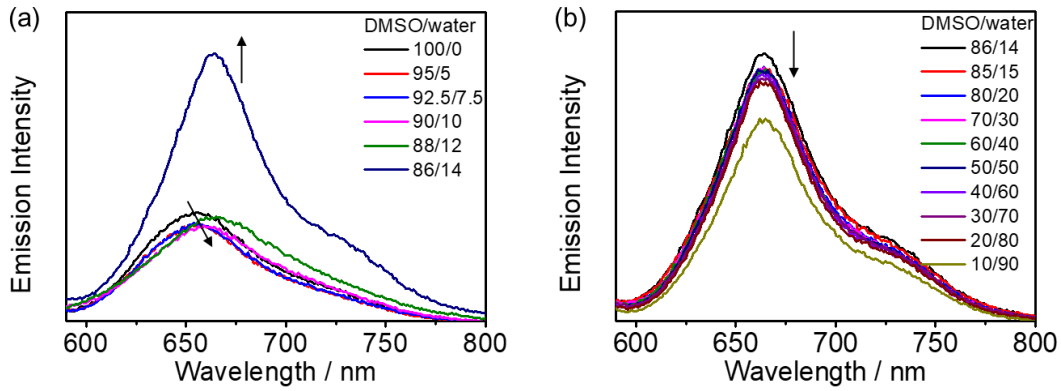

Figure S43. Emission spectral changes of **5** in DMSO solutions upon increasing water content from (a) 0 to 14 % and (b) 14 to 90 % in the concentration regime of 10^{-5} M.

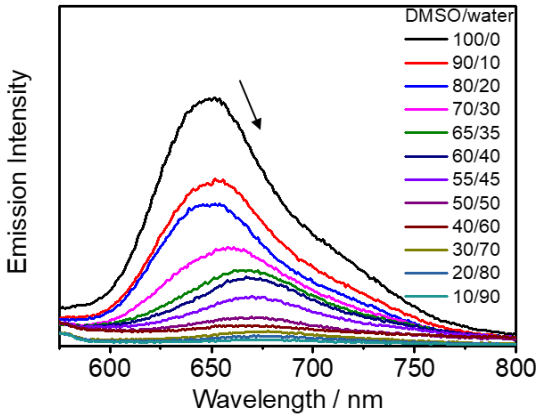

Figure S44. Emission changes of **6** in DMSO solutions upon increasing water content from 0 to 90 % in the concentration regime of 10^{-5} M.

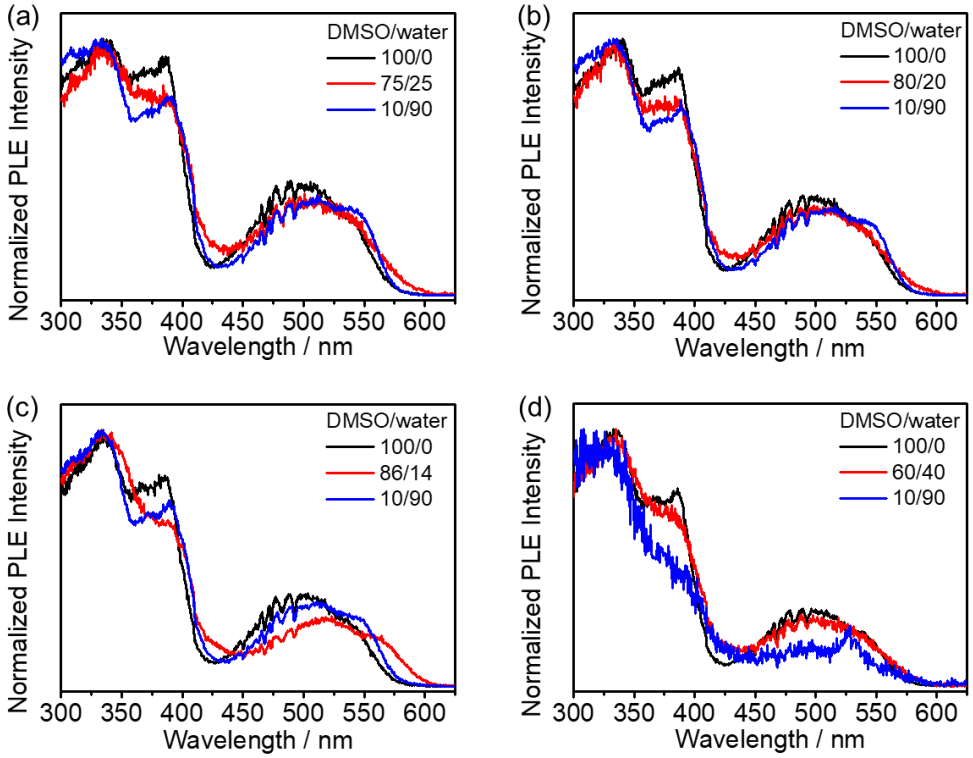

Figure S45. Normalized photoluminescence excitation (PLE) spectra of (a) **2** in DMSO, 25 % water–DMSO and 90 % water–DMSO solutions (v/v), (b) **3** in DMSO, 20 % water–DMSO and 90 % water–DMSO solutions (v/v), (c) **5** in DMSO, 14 % water–DMSO and 90 % water–DMSO solutions (v/v) and (d) **6** in DMSO, 40 % water–DMSO and 90 % water–DMSO solutions (v/v).

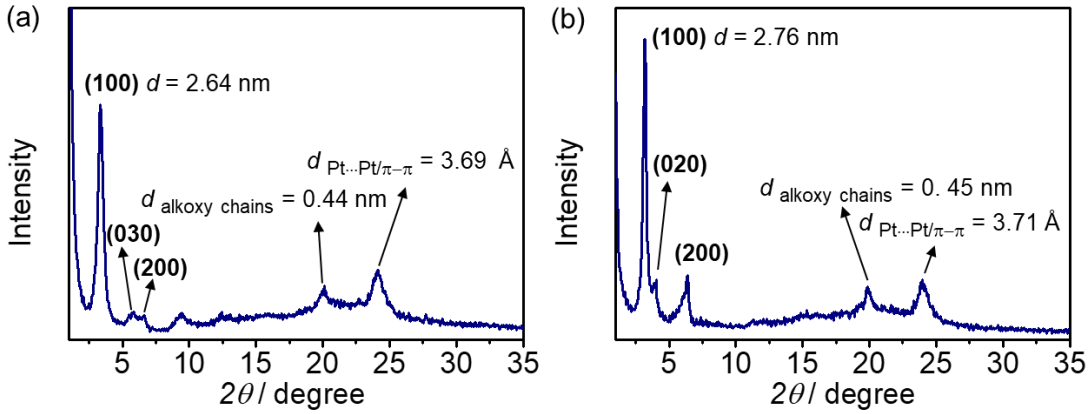

Figure S46. X-Ray diffraction (XRD) pattern of a thin film prepared from **2** in (a) 25 % water–DMSO solution and (b) 90 % water–DMSO solution.

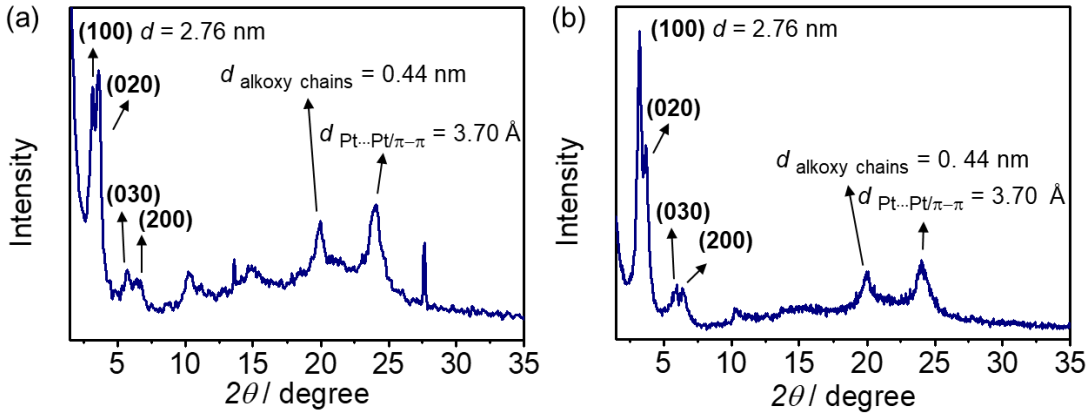

Figure S47. X-Ray diffraction (XRD) pattern of a thin film prepared from **3** in (a) 20 % water–DMSO solution and (b) 90 % water–DMSO solution.

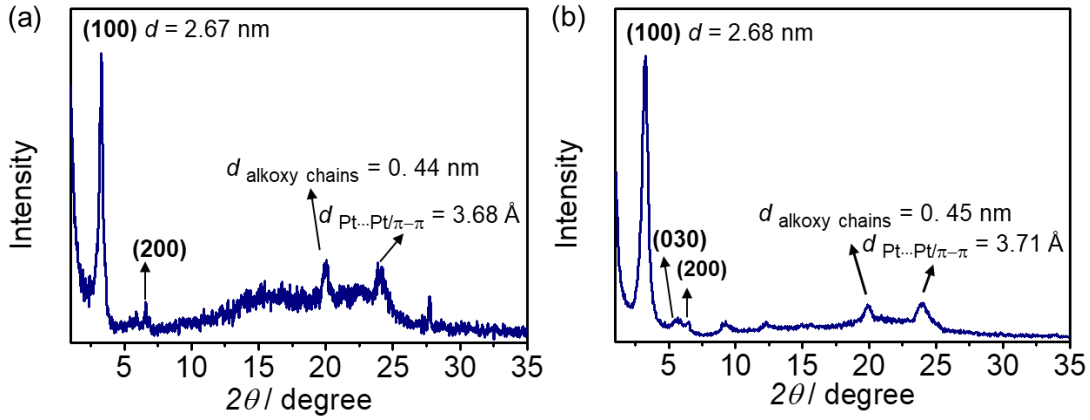

Figure S48. X-Ray diffraction (XRD) pattern of a thin film prepared from **4** in (a) 20 % water–DMSO solution and (b) 90 % water–DMSO solution.

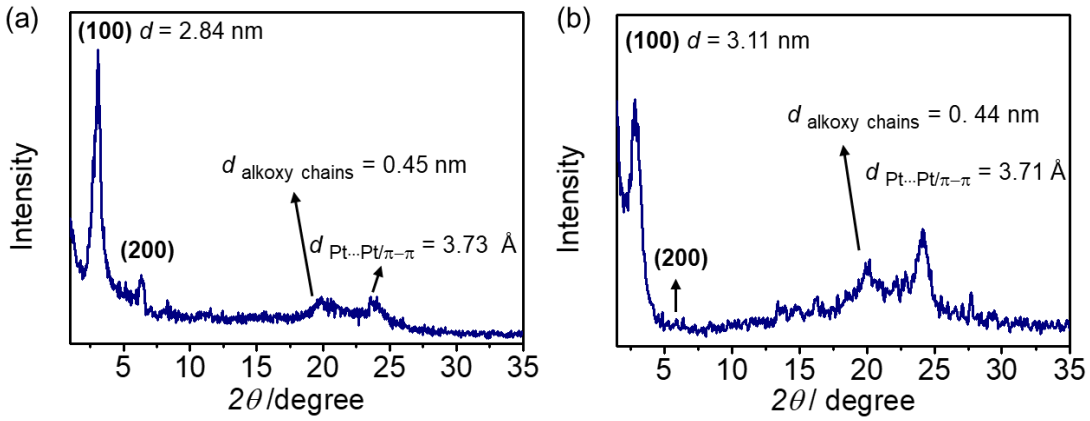

Figure S49. X-Ray diffraction (XRD) pattern of a thin film prepared from **5** in (a) 14 % water–DMSO solution and (b) 90 % water–DMSO solution.

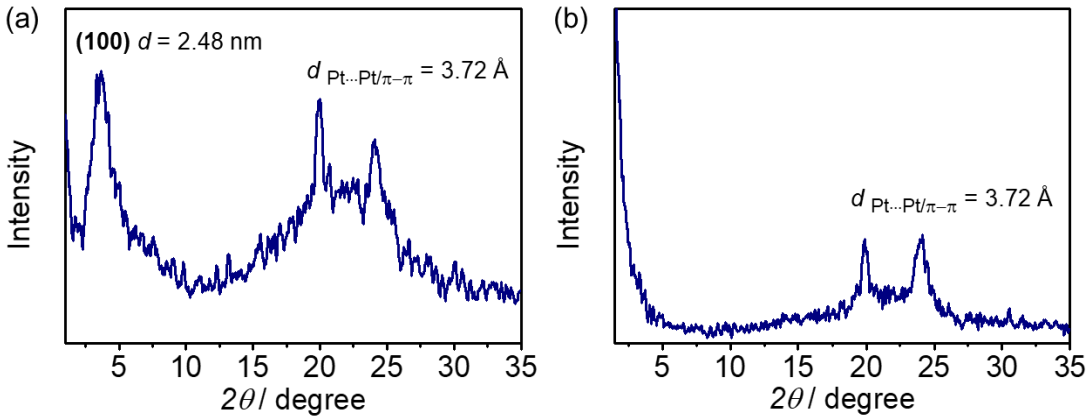

Figure S50. X-Ray diffraction (XRD) pattern of a thin film prepared from **6** in (a) 40 % water–DMSO solution and (b) 90 % water–DMSO solution.

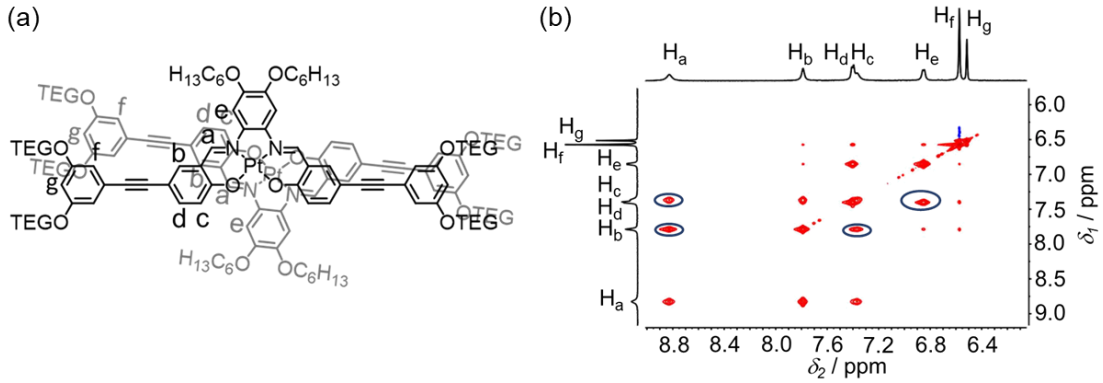

Figure S51. (a) Proposed stacking mode of **2** in DMSO upon an increase in H_2O content. (b) Partial ^1H–^1H NOESY NMR spectrum of **2** in DMSO-d_6 upon the addition of 5 % D_2O at 298 K.

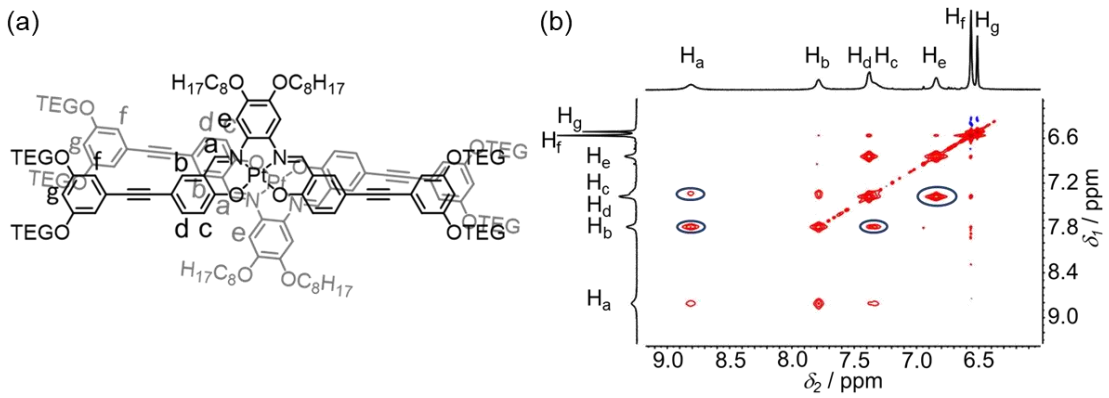

Figure S52. (a) Proposed stacking mode of **3** in DMSO upon an increase in H_2O content. (b) Partial ^1H–^1H NOESY NMR spectrum of **3** in DMSO-d_6 upon the addition of 5 % D_2O at 298 K.

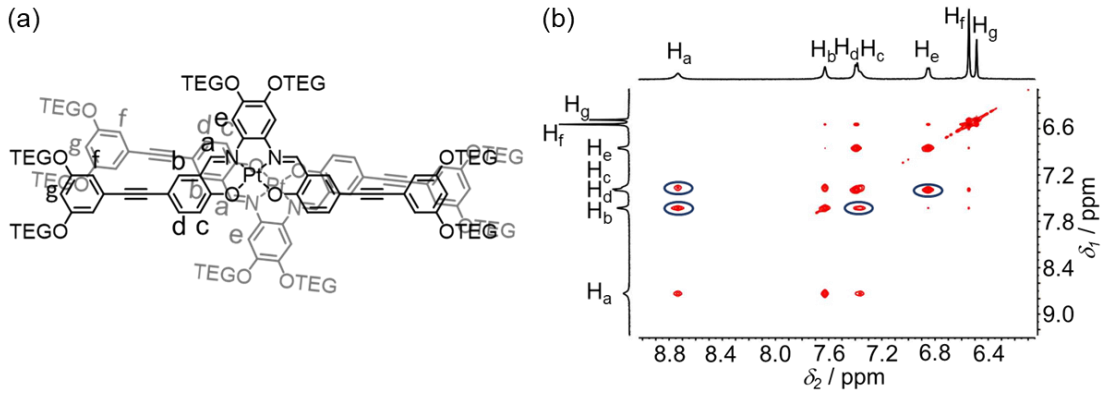

Figure S53. (a) Proposed stacking mode of **6** in DMSO upon an increase in H_2O content. (b) Partial ^1H–^1H NOESY NMR spectrum of **6** in DMSO-d_6 upon the addition of 5 % D_2O at 298 K.

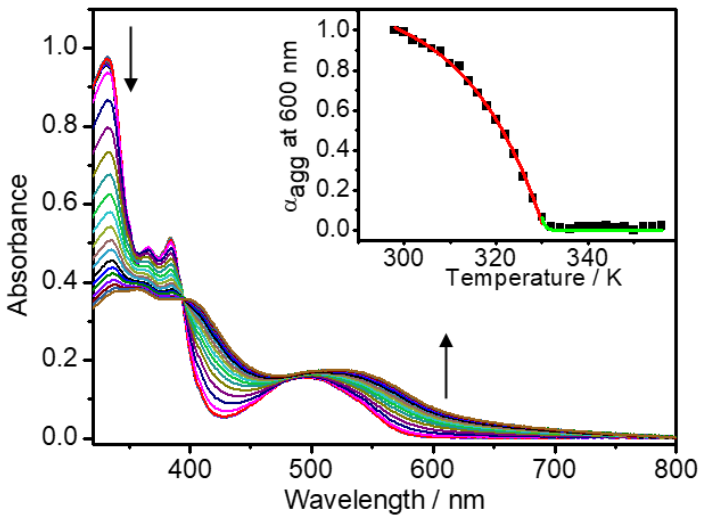

Figure S54. UV–Vis absorption spectral traces on cooling a solution of **2** in 25 % water–DMSO mixture at a cooling rate of 0.5 K min^{-1}. (Inset) A plot of degree of aggregation at 600 nm as a function of temperature with the curve fitted at the elongation (red line) and nucleation (green line) regime based on the nucleation–elongation model.

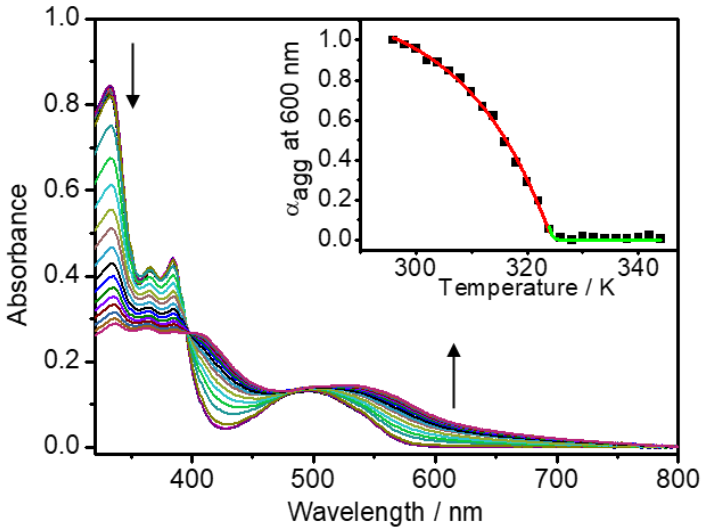

Figure S55. UV–Vis absorption spectral traces on cooling a solution of **3** in 20 % water–DMSO mixture at a cooling rate of 0.5 K min^{-1}. (Inset) A plot of degree of aggregation at 600 nm as a function of temperature with the curve fitted at the elongation (red line) and nucleation (green line) regime based on the nucleation−elongation model.

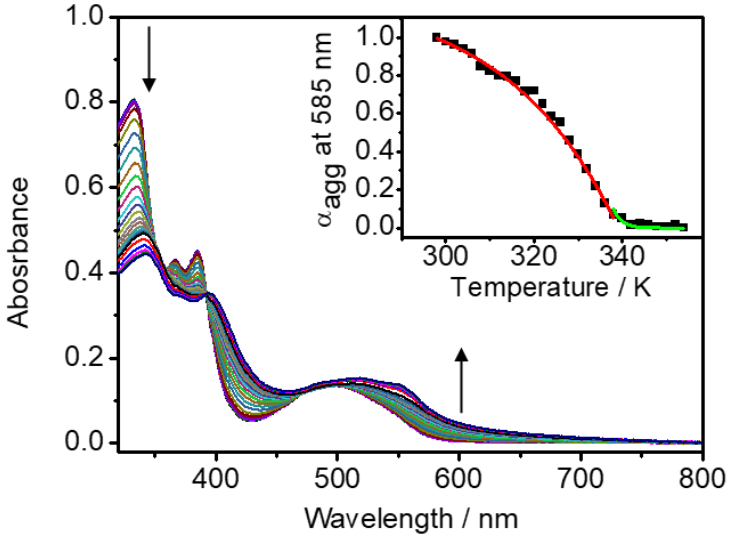

Figure S56. UV–Vis absorption spectral traces on cooling a solution of **5** in 14 % water–DMSO mixture at a cooling rate of 0.5 K min^{-1}. (Inset) A plot of degree of aggregation at 585 nm as a function of temperature with the curve fitted at the elongation (red line) and nucleation (green line) regime base on the nucleation−elongation model.

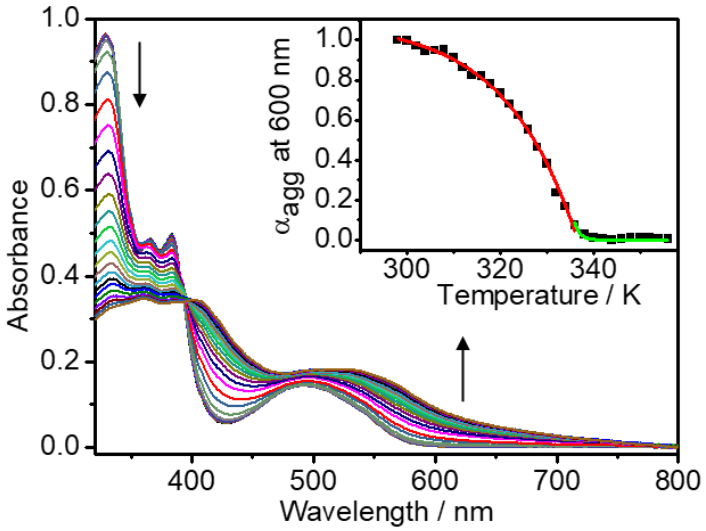

Figure S57. UV–Vis absorption spectral traces on cooling a solution of **6** in 40 % water–DMSO mixture at a cooling rate of 0.5 K min^{-1}. (Inset) A plot of degree of aggregation at 600 nm as a function of temperature with the curve fitted at the elongation (red line) and nucleation (green line) regime based on the nucleation−elongation model.

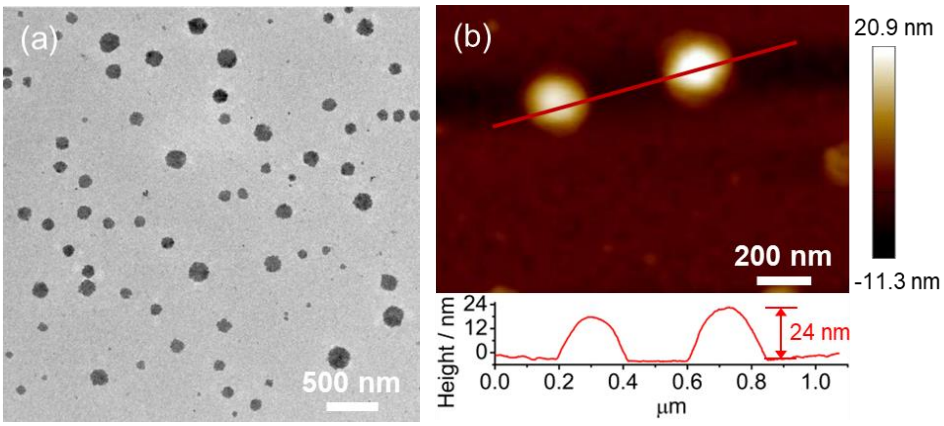

Figure S58. (a) TEM image and (b) AFM image prepared from a 25 % water–DMSO solution of **2** ([Pt] = 2.0×10^{-5} M).

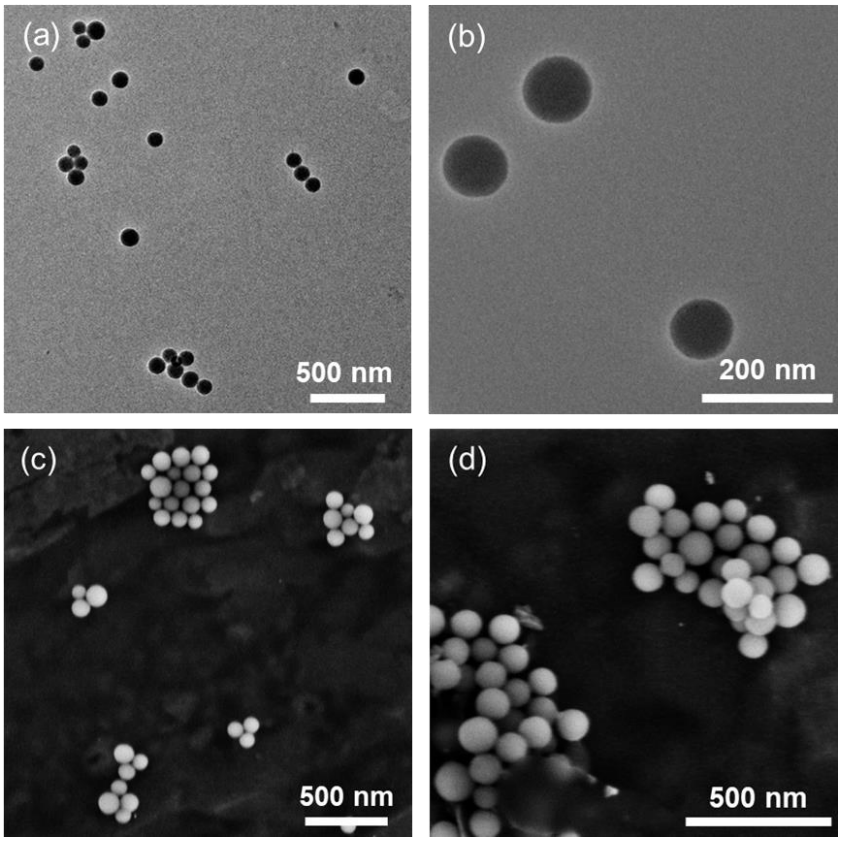

Figure S59. TEM images at (a) lower magnification and (b) higher magnification and SEM images at (c) lower magnification and (d) higher magnification images prepared from a 90 % water–DMSO solution of **2** ([Pt] = 2.0×10^{-5} M).

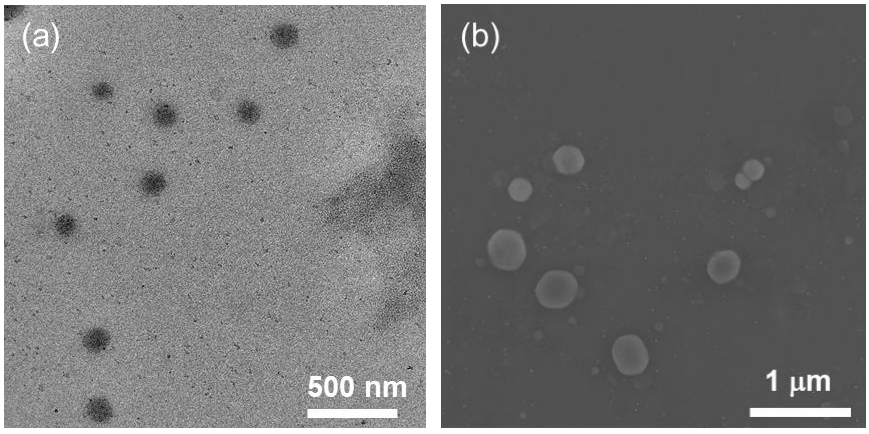

Figure S60. (a) TEM image and (b) SEM image prepared from a 20 % water–DMSO solution of **3** ([Pt] = 2.0×10^{-5} M).

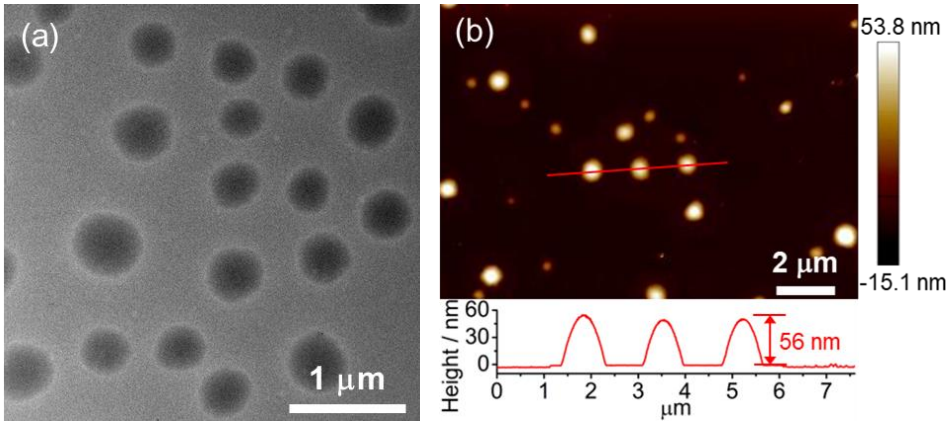

Figure S61. (a) TEM image and (b) AFM image prepared from a 90 % water–DMSO solution of **3** ([Pt] = 2.0×10^{-5} M).

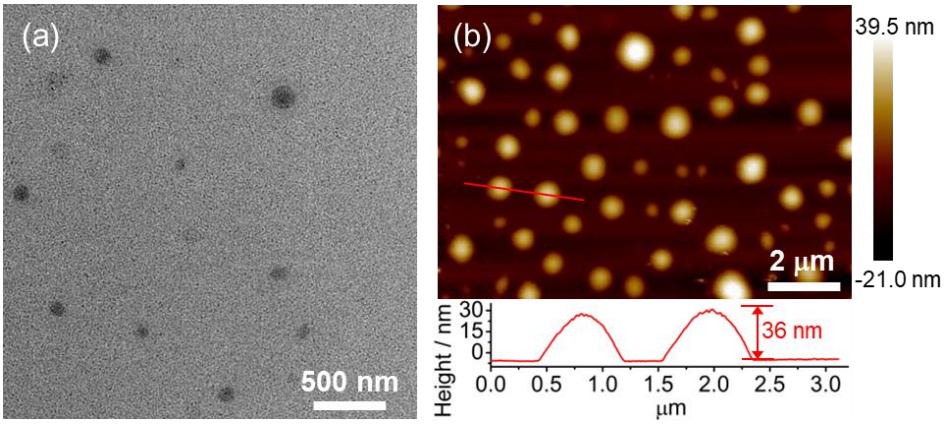

Figure S62. (a) TEM image and (b) AFM image prepared from a 40 % water–DMSO solution of **6** ([Pt] = 2.0×10^{-5} M).

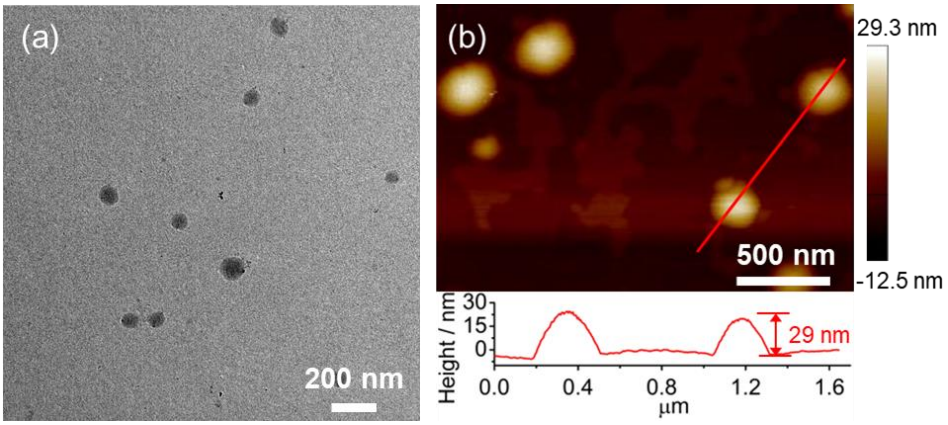

Figure S63. (a) TEM image and (b) AFM image prepared from a 90 % water–DMSO solution of **6** ([Pt] = 2.0×10^{-5} M).

Crystallographic Data

Table S1. Crystal and structure determination data of complex **1**

Empirical formula	$C_{48}H_{46}N_2O_8Pt$
Formula weight	973.99
Temperature	293(2) K
Wavelength	0.71073A
Crystal system, space group	Triclinic, $P\bar{1}$
Unit cell dimensions	a = 10.584(3) Å α = 84.579(11)°
	b = 13.174(4) Å β = 73.169(10)°
	c = 17.291(5) Å γ = 77.600(10)°
Volume	2252.4(11) Å^3
Z	2
Density(calculated)	1.561 mg m^{-3}
Absorption coefficient	3.290 mm^{-1}
F(000)	1064
Crystal size	0.130 × 0.120 × 0.100 mm^3
θ range for data collection	2.668 to 26.773°
Limiting indices	$-13 \le h \le 13$, $-16 \le k \le 16$, $-21 \le l \le 21$
Reflections collected / unique	119067 / 9583 [*R(int)* = 0.0594]
Completeness to θ = 25.242°	99.9 %
Absorption correction	Semi-empirical from equivalents
Max. and min. transmission	0.734 and 0.674
Refinement method	Full-matrix least-squares on F^2
Data / restraints / parameters	9583 / 125 / 638
Goodness-of-fit on F^2	1.048
Final *R* indices [$I > 2\sigma(I)$]	R_1 = 0.0277, wR_2 = 0.0604
R indices (all data)	R_1 = 0.0391, wR_2 = 0.0672
Extinction coefficient	n / a
Largest diff. peak and hole	1.668 and –0.979 eÅ^{-3}

Table S2. Selection bond lengths [Å], bond angles [°] and dihedral angles [°] with estimated standard deviations (esds) in parentheses for complex **1**

Pt(1)–N(1)	1.949(3)	Pt(1)–N(2)	1.963(3)
Pt(1)–O(1)	1.993(2)	Pt(1)–O(2)	1.991(2)
C(7)–N(1)	1.300(4)	C(38)–N(2)	1.302(4)
C(1)–O(1)	1.308(4)	C(32)–O(2)	1.314(4)
C(18)–N(1)	1.434(4)	C(23)–N(2)	1.418(4)
N(1)–Pt(1)–N(2)	83.82(11)	N(1)–Pt(1)–O(2)	179.46(10)
N(2)–Pt(1)–O(2)	95.68(10)	N(1)–Pt(1)–O(1)	95.54(10)
N(2)–Pt(1)–O(1)	178.93(11)	O(2)–Pt(1)–O(1)	84.96(9)
C(1)–O(1)–Pt(1)	123.1(2)	C(7)–N(1)–Pt(1)	124.2(2)
C(18)–N(1)–Pt(1)	112.7(2)	C(23)–N(2)–Pt(1)	112.8(2)
C(38)–N(2)–Pt(1)	123.8(2)	C(32)–O(2)–Pt(1)	123.1(2)
O(1)–C(1)–C(6)	125.6(3)	O(2)–C(32)–C(37)	125.5(3)
N(2)–C(38)–C(37)	126.0(3)	N(1)–C(7)–C(6)	125.9(3)
Plane C(1)–C(6)–Plane C(20)–C(15)	3.226(153)	Plane C(32)–C(37)–Plane C(41)–C(46)	7.239(164)

Photophysical data

Table S3. Photophysical data of complexes **1**–**6** in the degassed DMSO solutions (10^{-5} M) at 298 K

Complex	Absorption λ_{abs} / nm (ε / dm^3 mol^{-1} cm^{-1})	Emission λ_{em} / nm[a] (τ / μs; Φ_{em}[b])
1 (SBPt-C$_4$-Me)	334 (75070), 367 (39060), 385 (43370), 504 (12500), 540 sh (7590)	654[a] (1.14; 1.1×10^{-2})
2 (SBPt-C$_6$-TEG)	335 (106210), 367 (54830), 386 (60730), 505 (17610), 542 sh (10220)	653[a] (1.21; 1.5×10^{-2})
3 (SBPt-C$_8$-TEG)	335 (82780), 367 (42670), 386 (46700), 505 (13500), 539 sh (8330)	653[a] (1.15; 9.5×10^{-3})
4 (SBPt-C$_{12}$-TEG)	335 (88540), 367 (45340), 386 (50170), 505 (14590), 540 sh (8730)	654[a] (1.17; 9.7×10^{-3})
5 (SBPt-C$_{16}$-TEG)	334 (92760), 367 (50240), 386 (53980), 504 (15810), 542 sh (8900)	653[a] (1.21; 1.5×10^{-2})
6 (SBPt-TEG-TEG)	335 (96310), 367 (52790), 386 (55740), 505 (16350), 541 sh (9780)	641[a] (1.38; 1.7×10^{-2})

[a] Excitation wavelength at 480 nm in the degassed DMSO solution at 298 K. [b] Photoluminescence quantum yields (Φ_{em}) in degassed DMSO solution were determined with $[Ru(bpy)_3](PF_6)_2$ (bpy = 2,2'-bipyridine) in acetonitrile as a standard reference solution ($\Phi_{em} = 0.062$).

Table S4. Cartesian coordinates of the optimized S_0 state geometry of **7**.

C	3.449017	–2.77828	0.003491	C	0.648268	4.768147	0.002394
H	2.968406	–3.75179	0.003209	C	–0.77484	4.761747	–0.0017
O	–1.39123	–1.86514	–0.00309	C	–1.45713	3.557171	–0.00338
N	–1.35404	1.067143	–0.00239	H	–2.53879	3.561562	–0.00624
C	4.81619	–2.67222	0.003813	C	–0.75136	2.346862	–0.00148
H	5.428899	–3.56905	0.003786	C	2.63698	6.039263	0.009276
O	12.52135	–3.19204	–0.00607	H	3.059135	5.564754	–0.88446
O	1.220222	5.984112	0.004509	H	3.053067	5.563993	0.905446
C	4.646234	–0.27151	0.004218	C	–2.7749	6.014756	–0.00836
H	5.112019	0.710261	0.004481	H	–3.19277	5.536385	0.885337
O	11.98743	1.521389	0.002362	H	–3.18666	5.535914	–0.90464
C	5.450367	–1.40193	0.004052	C	–2.67325	–1.66075	–0.00373
O	–1.35777	5.972464	–0.00359	C	–3.50772	–2.80997	–0.00414
C	3.236121	–0.34706	0.003781	H	–3.0184	–3.77913	–0.00406
C	8.079327	–1.20548	0.002871	C	–4.87581	–2.71631	–0.00431
O	–12.5858	–3.27947	0.00698	H	–5.48037	–3.61864	–0.00436
C	6.865714	–1.29455	0.003663	C	–5.52137	–1.45174	–0.00428
O	–12.2411	1.354456	–0.0011	C	–4.72723	–0.31425	–0.00435
C	2.551988	0.906824	0.003605	H	–5.20196	0.663164	–0.00441
H	3.186516	1.790432	0.004384	C	–3.31658	–0.37694	–0.00405
C	9.498235	–1.09645	0.001499	C	–2.64411	0.883283	–0.00369
C	10.28223	–2.26748	–0.00136	H	–3.28702	1.760913	–0.00431
H	9.793699	–3.23366	–0.00226	C	–6.93745	–1.35615	–0.0037
C	11.49201	0.265022	0.001021	C	–8.15191	–1.27745	–0.00271
C	12.28054	–0.88196	–0.0019	C	–9.57102	–1.1743	–0.00111
H	13.36314	–0.83689	–0.00337	C	–10.3478	–2.34309	0.001857
C	11.66847	–2.14449	–0.0031	H	–9.85618	–3.30779	0.00266
C	10.09517	0.1651	0.002725	C	–11.74	–2.22606	0.003863
H	9.494005	1.06755	0.004879	C	–12.3433	–0.96782	0.002747
C	13.39585	1.672253	0.000599	H	–13.4252	–0.88719	0.004322
H	13.84736	1.228601	–0.8948	C	–11.5606	0.187315	–0.00029
H	13.84991	1.225827	0.893325	C	–10.1665	0.096633	–0.00225
H	13.58456	2.746911	0.001992	H	–9.53765	0.977978	–0.00449
C	11.96163	–4.49341	–0.00762	C	–11.4877	2.554265	–0.00432
H	11.35078	–4.66785	–0.9013	H	–10.8596	2.633694	–0.89958
H	11.35319	–4.67102	0.887093	H	–10.8568	2.636751	0.888671
H	12.80554	–5.18505	–0.00999	H	–12.2152	3.36747	–0.00456
C	1.341241	3.569638	0.003806	C	–12.0185	–4.57758	0.008592
H	2.422843	3.583693	0.006645	H	–11.4095	–4.75276	–0.88625
C	0.646196	2.353133	0.001636	H	–12.8586	–5.27379	0.01118
Pt	–0.04024	–0.39227	–0.0002	H	–11.4069	–4.74935	0.902257
C	2.604365	–1.63656	0.003197	H	2.895997	7.098659	0.010594
O	1.324215	–1.85244	0.002395	H	–3.04351	7.071766	–0.00956
N	1.26029	1.078866	0.002311				

Table S5. Cartesian coordinates of the optimized T_1 state geometry of **7**.

C	3.404842	–2.72662	0.003283	C	0.645361	4.835547	0.001494
H	2.885912	–3.68043	0.003123	C	–0.78216	4.827687	–0.00138
O	–1.37789	–1.74664	–0.00159	C	–1.4637	3.625653	–0.00236
N	–1.35903	1.149804	–0.00139	H	–2.54541	3.629586	–0.00437
C	4.779314	–2.67149	0.003596	C	–0.76039	2.406497	–0.00089
H	5.37012	–3.58146	0.003673	C	2.628882	6.113263	0.006137
O	12.46097	–3.32766	–0.00736	H	3.051571	5.638676	–0.88756
O	1.213291	6.055318	0.002875	H	3.047406	5.638333	0.90161
C	4.660388	–0.24558	0.003709	C	–2.7798	6.083152	–0.00634
H	5.164739	0.716495	0.003852	H	–3.1973	5.604156	0.887447
O	12.00797	1.393682	0.003346	H	–3.19291	5.60352	–0.90182
C	5.429971	–1.41206	0.003716	C	–2.674	–1.58839	–0.00224
O	–1.36369	6.040921	–0.0029	C	–3.45766	–2.76525	–0.00253
C	3.253612	–0.26892	0.003253	H	–2.92843	–3.71338	–0.00231
C	8.057982	–1.26469	0.002744	C	–4.83268	–2.72517	–0.00285
O	–12.5238	–3.4217	0.005681	H	–5.41334	–3.64166	–0.00288
C	6.841338	–1.33314	0.003436	C	–5.49731	–1.4732	–0.00303
O	–12.2519	1.21594	–0.00255	C	–4.74006	–0.29831	–0.00309
C	2.583392	0.985043	0.002967	H	–5.25481	0.658237	–0.00328
H	3.215152	1.86772	0.003413	C	–3.33355	–0.30653	–0.00264
C	9.475339	–1.18156	0.001413	C	–2.67747	0.955501	–0.00245
C	10.23746	–2.36752	–0.00197	H	–3.32	1.830425	–0.00295
H	9.731079	–3.32439	–0.00323	C	–6.90904	–1.40808	–0.00277
C	11.48995	0.14751	0.001448	C	–8.12642	–1.34985	–0.00216
C	12.25692	–1.01453	–0.00207	C	–9.54345	–1.27006	–0.00122
H	13.34018	–0.98786	–0.00366	C	–10.3003	–2.45279	0.001453
C	11.62501	–2.26786	–0.00381	H	–9.79209	–3.4088	0.002494
C	10.09215	0.07145	0.003158	C	–11.6935	–2.35745	0.002861
H	9.504792	0.982838	0.005719	C	–12.3147	–1.10726	0.001401
C	13.41945	1.519363	0.001623	H	–13.3978	–1.04346	0.002519
H	13.86242	1.06821	–0.89417	C	–11.5518	0.06177	–0.00137
H	13.86495	1.06453	0.894296	C	–10.1572	–0.00689	–0.00268
H	13.62688	2.590437	0.003534	H	–9.54065	0.883026	–0.00469
C	11.8805	–4.62043	–0.0097	C	–11.5187	2.428908	–0.00545
H	11.26704	–4.78394	–0.90356	H	–10.8919	2.518355	–0.90057
H	11.26967	–4.78837	0.885134	H	–10.8899	2.521437	0.887945
H	12.71347	–5.32506	–0.01267	H	–12.2602	3.229282	–0.00599
C	1.339928	3.641104	0.002597	C	–11.9376	–4.71196	0.007782
H	2.42154	3.656861	0.0046	H	–11.326	–4.87783	–0.88695
C	0.649844	2.414027	0.00125	H	–12.7677	–5.4199	0.010178
Pt	–0.04022	–0.29192	0.000288	H	–11.3241	–4.87403	0.901886
C	2.608452	–1.55841	0.002929	H	2.886882	7.173037	0.006938
O	1.314163	–1.73103	0.002286	H	–3.0495	7.140009	–0.00737
N	1.261868	1.164422	0.001862				

Table S6. Cartesian coordinates of the optimized S_0 state geometry of the dimer $\mathbf{7}_2$.

C	–3.25364	2.820716	–1.71234	O	–1.55694	–1.89127	1.697891
H	–2.76937	3.79215	–1.72792	N	–1.52088	1.044416	1.571837
O	1.556935	1.890998	–1.69691	C	4.622628	–2.72061	1.651604
N	1.520846	–1.04469	–1.57089	H	5.22984	–3.6202	1.618729
C	–4.62267	2.72037	–1.65122	O	12.35373	–3.07361	1.012399
H	–5.22988	3.619958	–1.61848	O	1.070255	5.921529	1.018049
O	–12.3541	3.073564	–1.01566	C	4.457191	–0.31995	1.668121
O	–1.07031	–5.92176	–1.01687	H	4.925114	0.659583	1.639655
C	–4.45723	0.319707	–1.66768	O	11.75012	1.523936	2.057156
H	–4.92517	–0.65982	–1.63931	C	5.257802	–1.45355	1.634972
O	–11.75	–1.52442	–2.05815	O	–1.50596	5.912068	0.957849
C	–5.25785	1.453317	–1.63473	C	3.049964	–0.3908	1.712543
O	1.505911	–5.91233	–0.95681	C	7.882193	–1.22078	1.555438
C	–3.04999	0.390553	–1.71184	O	–12.7816	–3.13882	0.908332
C	–7.88227	1.220555	–1.55611	C	6.671348	–1.33619	1.581675
O	12.781	3.140309	–0.90873	O	–12.3507	1.348461	2.06899
C	–6.67142	1.335947	–1.58187	C	2.376563	0.870231	1.651555
O	12.35175	–1.34648	–2.07179	H	3.021848	1.743247	1.590851
C	–2.3766	–0.87048	–1.6507	C	9.298488	–1.08704	1.550077
H	–3.0219	–1.74348	–1.59007	C	10.09992	–2.21359	1.279297
C	–9.29858	1.086808	–1.55125	H	9.628452	–3.16682	1.077514
C	–10.1001	2.213468	–1.28127	C	11.27	0.279328	1.802223
H	–9.62876	3.166788	–1.07968	C	12.07712	–0.82408	1.544931
C	–11.27	–0.2797	–1.80357	H	13.158	–0.75652	1.526477
C	–12.0772	0.823812	–1.54709	C	11.4823	–2.06359	1.275687
H	–13.1581	0.756239	–1.52904	C	9.876577	0.156366	1.810398
C	–11.4825	2.063447	–1.27815	H	9.262351	1.027661	2.007448
C	–9.87654	–0.15672	–1.81126	C	13.15941	1.692638	2.088689
H	–9.26222	–1.02808	–2.00769	H	13.61153	1.082061	2.878259
C	–13.1592	–1.69316	–2.09008	H	13.61426	1.439733	1.125551
H	–13.6111	–1.08294	–2.88007	H	13.33021	2.748055	2.303389
H	–13.6144	–1.43985	–1.12721	C	11.81694	–4.37742	0.847719
H	–13.33	–2.74868	–2.30438	H	11.27731	–4.69848	1.745765
C	–11.8174	4.377472	–0.85137	H	11.14781	–4.43297	–0.01744
H	–11.2771	4.697973	–1.7492	H	12.67179	–5.03433	0.683276
H	–11.1489	4.433544	0.01428	C	1.184229	3.525489	1.360008
H	–12.6724	5.034487	–0.68801	H	2.265908	3.538777	1.375913
C	–1.18427	–3.52573	–1.35889	C	0.482204	2.322167	1.5014
H	–2.26595	–3.53902	–1.37474	Pt	–0.21466	–0.41081	1.688602
C	–0.48225	–2.32242	–1.50034	C	2.41903	–1.67622	1.746218
Pt	0.214637	0.410549	–1.68758	O	1.130461	–1.88451	1.795792
C	–2.41905	1.675974	–1.74546	N	1.088521	1.052355	1.641212
O	–1.13047	1.884257	–1.79494	C	0.492649	4.710417	1.178885
N	–1.08856	–1.05261	–1.6402	C	–0.92707	4.7058	1.14829
C	–0.4927	–4.71066	–1.17776	C	–1.61796	3.51707	1.301806

C	0.927018	–4.70606	–1.14723	H	–2.69889	3.523077	1.271638
C	1.617915	–3.51734	–1.30079	C	–0.91519	2.3181	1.469419
H	2.698848	–3.52336	–1.27065	C	2.490345	5.970482	1.020563
C	0.915149	–2.31836	–1.4684	H	2.896161	5.621721	1.976585
C	–2.4904	–5.97071	–1.01944	H	2.907788	5.370692	0.203969
H	–2.89618	–5.62195	–1.97547	C	–2.92551	5.950455	0.903239
H	–2.90787	–5.37092	–0.20286	H	–3.30598	5.34127	0.075732
C	2.925462	–5.95073	–0.90222	H	–3.36628	5.606281	1.845332
H	3.305954	–5.34151	–0.07475	C	–2.84375	–1.68685	1.601776
H	3.366223	–5.6066	–1.84433	C	–3.67134	–2.83465	1.52626
C	2.843758	1.686556	–1.60095	H	–3.18235	–3.80395	1.539183
C	3.671369	2.834341	–1.52546	C	–5.03976	–2.74019	1.449766
H	3.18238	3.803645	–1.53826	H	–5.64224	–3.642	1.398753
C	5.039795	2.739864	–1.44918	C	–5.68228	–1.47656	1.448158
H	5.642286	3.641667	–1.3982	C	–4.88717	–0.33913	1.495787
C	5.682311	1.476232	–1.44775	H	–5.36018	0.638156	1.473336
C	4.88718	0.338809	–1.49532	C	–3.48	–0.40416	1.563842
H	5.360189	–0.63848	–1.47298	C	–2.80841	0.858642	1.530325
C	3.480003	0.403854	–1.56316	H	–3.45249	1.731199	1.450348
C	2.808387	–0.85893	–1.52956	C	–7.09763	–1.37248	1.418817
H	3.452466	–1.7315	–1.44969	C	–8.311	–1.28261	1.431244
C	7.097676	1.372204	–1.41865	C	–9.72798	–1.16321	1.469948
C	8.311058	1.282563	–1.43131	C	–10.5253	–2.27689	1.16826
C	9.728076	1.163683	–1.47045	H	–10.0539	–3.21538	0.906249
C	10.52497	2.27755	–1.16844	C	–11.913	–2.13494	1.200582
H	10.05328	3.215704	–0.9058	C	–12.4958	–0.91252	1.529802
C	11.91279	2.136216	–1.20128	H	–13.5758	–0.80987	1.536538
C	12.49604	0.914235	–1.53137	C	–11.6892	0.189901	1.811557
H	13.576	0.812068	–1.53857	C	–10.2996	0.075587	1.798742
C	11.68975	–0.18838	–1.81345	H	–9.65495	0.917616	2.014514
C	10.30016	–0.07471	–1.80004	C	–11.5688	2.501868	2.339898
H	9.655771	–0.91692	–2.01597	H	–11.0035	2.386482	3.271639
C	11.57035	–2.50005	–2.34335	H	–10.8755	2.71555	1.520021
H	11.00416	–2.38395	–3.27448	H	–12.275	3.326419	2.443174
H	10.87791	–2.71512	–1.52312	C	–12.236	–4.34406	0.393763
H	12.27694	–3.32407	–2.44816	H	–11.611	–4.85081	1.137491
C	12.23503	4.345008	–0.39329	H	–13.0884	–4.97857	0.14849
H	11.6096	4.85192	–1.13652	H	–11.6476	–4.15582	–0.51111
H	13.08723	4.979753	–0.14792	H	–3.1891	6.995206	0.738307
H	11.64705	4.155985	0.511672	H	2.752631	7.018347	0.874318
C	3.253613	–2.82096	1.712988	H	3.189045	–6.99548	–0.73725
H	2.769341	–3.79239	1.728654	H	–2.7527	–7.01858	–0.8732

Table S7. Cartesian coordinates of the optimized T_1 state geometry of the dimer $\mathbf{7}_2$.

C	–3.19976	2.827481	–1.66066	O	–1.531	–1.80538	1.676307
H	–2.70025	3.791246	–1.66764	N	–1.5558	1.140797	1.580812
O	1.602354	1.809797	–1.64037	C	4.648689	–2.56525	1.655965
N	1.508784	–1.1244	–1.53594	H	5.260577	–3.46069	1.614095
C	–4.57053	2.748988	–1.60386	O	12.38929	–2.91606	1.450317
H	–5.16324	3.658026	–1.56571	O	0.944224	5.974126	0.818026
O	–12.3343	3.073994	–0.88034	C	4.471621	–0.15915	1.73235
O	–1.17581	–5.95645	–1.03913	H	4.941563	0.820019	1.735729
C	–4.44193	0.346481	–1.64468	O	11.73857	1.774271	1.846389
H	–4.92584	–0.62532	–1.6281	C	5.271967	–1.29068	1.688266
O	–11.702	–1.46815	–2.12836	O	–1.59521	5.940586	0.883224
C	–5.22508	1.491874	–1.59824	C	3.054369	–0.22049	1.74171
O	1.398542	–5.99287	–0.93703	C	7.896596	–1.04662	1.662664
C	–3.03427	0.394232	–1.68492	O	–12.7537	–3.22261	0.750381
C	–7.85061	1.274062	–1.51171	C	6.685639	–1.16756	1.666603
O	12.83982	2.927809	–1.33804	O	–12.3616	1.20973	2.117888
C	–6.63976	1.389271	–1.5423	C	2.388879	1.023496	1.708503
O	12.35575	–1.67118	–1.87856	H	3.012697	1.910817	1.717432
C	–2.38486	–0.8794	–1.6372	C	9.311372	–0.90303	1.670415
H	–3.04648	–1.74133	–1.59691	C	10.12481	–2.04906	1.567178
C	–9.26636	1.133246	–1.50609	H	9.662715	–3.02483	1.488627
C	–10.0748	2.241916	–1.18663	C	11.26929	0.502744	1.760301
H	–9.60952	3.188919	–0.945	C	12.08768	–0.61818	1.666036
C	–11.2296	–0.23356	–1.81713	H	13.16813	–0.54371	1.651623
C	–12.0435	0.852413	–1.51171	C	11.50589	–1.88838	1.561573
H	–13.1239	0.777352	–1.49569	C	9.87694	0.369528	1.76793
C	–11.4563	2.082633	–1.18843	H	9.253299	1.25388	1.832609
C	–9.83698	–0.10183	–1.81838	C	13.14665	1.954877	1.866721
H	–9.21729	–0.95954	–2.05412	H	13.59339	1.468485	2.741071
C	–13.1102	–1.64028	–2.18141	H	13.61287	1.566889	0.955353
H	–13.5569	–0.99534	–2.94645	H	13.31048	3.031247	1.927411
H	–13.5758	–1.43356	–1.21243	C	11.86615	–4.23554	1.457912
H	–13.2747	–2.68526	–2.44616	H	11.31416	–4.4363	2.382965
C	–11.8063	4.371921	–0.65355	H	11.21248	–4.41654	0.598237
H	–11.2695	4.739608	–1.53524	H	12.72905	–4.89985	1.398835
H	–11.1372	4.390517	0.213219	C	1.142726	3.618426	1.249433
H	–12.6655	5.014284	–0.4574	H	2.222721	3.640776	1.204757
C	–1.24229	–3.55617	–1.36072	C	0.461432	2.401106	1.464626
H	–2.32363	–3.54971	–1.38885	Pt	–0.22311	–0.29783	1.678884
C	–0.51752	–2.36409	–1.48269	C	2.438305	–1.52553	1.732562
Pt	0.229807	0.356524	–1.64104	O	1.146607	–1.74517	1.769107
C	–2.38232	1.669594	–1.69744	N	1.047615	1.198561	1.651623
O	–1.09024	1.85792	–1.73402	C	0.426666	4.771907	1.0552
N	–1.09968	–1.08401	–1.61734	C	–1.03375	4.753414	1.084722
C	–0.57443	–4.75442	–1.18152	C	–1.71597	3.575668	1.289531

C	0.844694	–4.77507	–1.12942	H	–2.79669	3.57785	1.288828
C	1.558854	–3.59798	–1.26561	C	–1.00177	2.380301	1.454524
H	2.639043	–3.62385	–1.22097	C	2.364965	6.088711	0.753719
C	0.879771	–2.38525	–1.43624	H	2.817607	5.791615	1.704674
C	–2.5962	–5.97992	–1.06876	H	2.76263	5.472984	–0.05913
H	–2.97726	–5.61735	–2.02985	C	–3.02113	6.014821	0.871056
H	–3.01828	–5.37812	–0.25614	H	–3.4295	5.393552	0.068102
C	2.8142	–6.05358	–0.83184	H	–3.42921	5.698871	1.835658
H	3.173207	–5.45255	0.011398	C	–2.82658	–1.63373	1.577046
H	3.294583	–5.71343	–1.75592	C	–3.61818	–2.80079	1.470192
C	2.886827	1.579013	–1.57402	H	–3.09784	–3.75394	1.460249
C	3.739859	2.709718	–1.52386	C	–4.99139	–2.75269	1.390896
H	3.270964	3.689075	–1.5238	H	–5.56548	–3.67058	1.312705
C	5.107483	2.58713	–1.48929	C	–5.66723	–1.50579	1.424253
H	5.729912	3.476283	–1.45902	C	–4.91019	–0.34656	1.509528
C	5.723963	1.310381	–1.50304	H	–5.41617	0.614255	1.514358
C	4.904382	0.189581	–1.52187	C	–3.49517	–0.35878	1.573653
H	5.356525	–0.79788	–1.5087	C	–2.87505	0.914386	1.564081
C	3.49762	0.283617	–1.55158	H	–3.53835	1.772004	1.514866
C	2.800869	–0.96429	–1.50374	C	–7.08469	–1.43554	1.389211
H	3.427695	–1.8495	–1.43296	C	–8.29942	–1.36223	1.393962
C	7.137043	1.178868	–1.51091	C	–9.71749	–1.25579	1.425916
C	8.348081	1.06593	–1.54882	C	–10.5051	–2.35947	1.067633
C	9.762559	0.925427	–1.59878	H	–10.0254	–3.28188	0.766437
C	10.57356	2.061276	–1.45934	C	–11.894	–2.22788	1.095544
H	10.11304	3.03117	–1.32238	C	–12.4875	–1.02549	1.475714
C	11.95944	1.902081	–1.48421	H	–13.5681	–0.9303	1.478838
C	12.52777	0.640222	–1.64889	C	–11.6904	0.068231	1.813484
H	13.60654	0.525958	–1.6493	C	–10.3001	–0.0365	1.805508
C	11.7078	–0.48122	–1.77454	H	–9.66242	0.798664	2.064476
C	10.3195	–0.35194	–1.76537	C	–11.5900	2.353655	2.450988
H	9.66555	–1.20926	–1.85771	H	–11.0332	2.19751	3.381916
C	11.55924	–2.84212	–1.97596	H	–10.8899	2.610421	1.649461
H	10.98288	–2.85248	–2.90802	H	–12.3025	3.168141	2.58591
H	10.87478	–2.93023	–1.12615	C	–12.1963	–4.39837	0.182813
H	12.25585	–3.68117	–1.97083	H	–11.5721	–4.93531	0.905761
C	12.30914	4.197098	–0.98764	H	–13.0426	–5.02647	–0.09746
H	11.6834	4.604765	–1.7894	H	–11.6039	–4.16346	–0.70841
H	13.16906	4.850423	–0.83583	H	–3.25812	7.06216	0.690611
H	11.72563	4.139139	–0.06222	H	2.566059	7.140791	0.557377
C	3.275278	–2.66303	1.682821	H	3.055773	–7.10275	–0.66134
H	2.790236	–3.63448	1.665762	H	–2.8800	–7.02381	–0.93485

Table S8. The first twenty singlet (S_n) excited states computed by TDDFT/SMD (**7**: DMSO, $\mathbf{7}_2$: water) at the optimized ground–state geometries for the complexes described.

Complex	S_n	Excitation[a] (Coefficient)[b]	Vertical excitation wavelength / nm	f [c]
7	S_1	H→L (0.69)	503	0.100
	S_2	H−1→L (0.69)	479	0.347
	S_3	H→L+1 (0.59)	391	0.000
		H−2→L (0.36)		
	S_4	H−2→L (0.59)	384	0.597
		H→L+1 (−0.35)		
	S_5	H–1→L+1 (0.63)	371	0.275
	S_6	H–3→L (0.57)	351	0.088
		H–5→L (−0.33)		
	S_7	H–5→L (0.53)	346	0.102
		H–3→L (0.40)		
	S_8	H–4→L (0.70)	338	0.001
	S_9	H–8→L (0.70)	335	0.000
	S_{10}	H→L+2 (0.48)	334	2.921
		H–6→L (0.32)		
	S_{11}	H–6→L (0.52)	328	0.054
		H→L+2 (−0.35)		
	S_{12}	H−2→L+1 (0.43)	323	0.057
		H→L+3 (0.42)		
	S_{13}	H−2→L+1 (0.49)	319	0.030
		H→L+3 (−0.36)		
	S_{14}	H−1→L+2 (0.62)	307	0.044
	S_{15}	H−1→L+3 (0.56)	305	0.061
		H→L+3 (−0.32)		
	S_{16}	H–7→L (0.60)	304	0.206
	S_{17}	H–11→L (0.70)	302	0.000
	S_{18}	H–9→L (0.58)	297	0.019
	S_{19}	H→L+5 (0.59)	296	0.000
	S_{20}	H–5→L+1 (0.45)	293	0.037
		H–3→L+1 (–0.40)		

7$_2$	S_1	H→L (0.68)	525	0.000
	S_2	H−2→L (0.52)	497	0.122
		H→L+1 (0.45)		
	S_3	H−3→L (0.68)	489	0.000
	S_4	H−1→L (0.66)	486	0.061
	S_5	H→L+1 (0.52)	483	0.017
		H–2→L (–0.45)		
	S_6	H−2→L+1 (0.68)	466	0.000
	S_7	H−1→L+1 (0.66)	458	0.000
	S_8	H−3→L+1 (0.68)	454	0.338
	S_9	H−4→L (0.67)	414	0.498
	S_{10}	H−4→L+1 (0.67)	403	0.000
	S_{11}	H–11→L (0.62)	401	0.014
	S_{12}	H→L+2 (0.61)	392	0.000
	S_{13}	H→L+3 (0.59)	391	0.156
	S_{14}	H–11→L+1 (0.57)	383	0.000
	S_{15}	H–5→L (0.45)	381	0.000
		H–6→L (0.38)		
	S_{16}	H–2→L+2 (0.58)	376	0.011
	S_{17}	H–3→L+2 (0.42)	376	0.000
		H–1→L+3 (0.32)		
		H–10→L (–0.30)		
	S_{18}	H−1→L+2 (0.54)	371	0.218
	S_{19}	H–2→L+3 (0.56)	371	0.001
	S_{20}	H–3→L+3 (0.57)	366	0.066
		H–1→L+2 (–0.34)		

[a] The orbitals involved in the excitation (H = HOMO and L = LUMO).

[b] The coefficients in the configuration interaction (CI) expansion that are less than 0.3 are not listed.

[c] Oscillator strengths.

Table S9. Dynamic light scattering data of complexes **2**–**6** in various solvent compositions at 298 K

Complex	Medium	Hydrodynamic diameter / nm
2 (SBPt-C_6-TEG)	DMSO	_[a]
	25 % water–DMSO (v/v)	275.5[b], _[d]
	90 % water–DMSO (v/v)	91.35[b], _[d]
3 (SBPt-C_8-TEG)	DMSO	_[a]
	20 % water–DMSO (v/v)	198.2[b], _[d]
	90 % water–DMSO (v/v)	401.4[b], _[d]
4 (SBPt-C_{12}-TEG)	DMSO	_[a]
	20 % water–DMSO (v/v)	171.0[b], _[d]
	90 % water–DMSO (v/v)	74.23, 1588[b], _[d]
5 (SBPt-C_{16}-TEG)	DMSO	_[a]
	14 % water–DMSO (v/v)	141.2, 4790[b], _[d]
	90 % water–DMSO (v/v)	64.01[b], _[d]
6 (SBPt-TEG-TEG)	DMSO	_[a]
	40 % water–DMSO (v/v)	184.3[b], _[d]
	90 % water–DMSO (v/v)	97.79[b], _[d]
	water	47.56[c]

[a] No scattering signals.

[b] At a concentration of 2.0×10^{-5} M.

[c] At a concentration of 2.0×10^{-4} M.

[d] At a concentration of 2.0×10^{-5} M at 363 K.

References

1 Gaussian 16, Revision C.01,M. J. Frisch, G. W. Trucks, H. B. Schlegel, G. E. Scuseria, M. A. Robb, J. R. Cheeseman, G. Scalmani, V. Barone, G. A. Petersson, H. Nakatsuji, X. Li, M. Caricato, A. V. Marenich, J. Bloino, B. G. Janesko, R. Gomperts, B. Mennucci, H. P. Hratchian, J. V. Ortiz, A. F. Izmaylov, J. L. Sonnenberg, D. Williams-Young, F. Ding, F. Lipparini, F. Egidi, J. Goings, B. Peng, A. Petrone, T. Henderson, D. Ranasinghe, V. G. Zakrzewski, J. Gao, N. Rega, G. Zheng, W. Liang, M. Hada, M. Ehara, K. Toyota, R. Fukuda, J. Hasegawa, M. Ishida, T. Nakajima, Y. Honda, O. Kitao, H. Nakai, T. Vreven, K. Throssell, J. A. Montgomery, Jr, J. E. Peralta, F. Ogliaro, M. J. Bearpark, J. J. Heyd, E. N. Brothers, K. N. Kudin, V. N. Staroverov, T. A. Keith, R. Kobayashi, J. Normand, K. Raghavachari, A. P. Rendell, J. C. Burant, S. S. Iyengar, J. Tomasi, M. Cossi, J. M. Millam, M. Klene, C. Adamo, R. Cammi, J. W. Ochterski, R. L. Martin, K. Morokuma, O. Farkas, J. B. Foresman and D. J. Fox, Gaussian, Inc., Wallingford CT, 2019.

2 J. P. Perdew, M. Ernzerhof and K. Burke, Rationale for Mixing Exact Exchange with Density Functional Approximations, *J. Chem. Phys.*, 1996, **105**, 9982.

3 C. Adamo and V. Barone, Toward Reliable Density Functional Methods without Adjustable Parameters: The PBE0 Model, *J. Chem. Phys.*, 1999, **110**, 6158.

4 A. V. Marenich, C. J. Cramer and D. G. Truhlar, Universal Solvation Model Based on Solute Electron Density and on a Continuum Model of the Solvent Defined by the Bulk Dielectric Constant and Atomic Surface Tensions, *J. Phys. Chem. B*, 2009, **113**, 6378.

5 D. Andrae, U. H/iuBermann, M. Dolg, H. Stoll, H. PreuB, Energy-Adjusted *ab Initio* Pseudopotentials for the Second and Third Row Transition Elements, *Theor. Chim, Acta*, 1990, **77**, 123.

6 A.W. Ehlers, M. Böhme, S. Dapprich, A. Gobbi, A. Hijllwarth, V. Jonas, K.F. Köhler, R. Stegmann, A. Veldkamp and G. Frenking, A Set of f-Polarization Functions for Pseudo-Potential Basis Sets of the Transition Metals Sc–Cu, Y–Ag and La–Au, *Chem. Phys. Lett.*, 1993, **208**, 111.

7 P. C. Hariharan and J. A. Pople, The Influence of Polarization Functions on Molecular Orbital Hydrogenation Energies, *Theoret. Chim. Acta*, 1973, **28**, 213.

8 J. D. Dill and J. A. Pople, Self‐Consistent Molecular Orbital Methods. XV. Extended Gaussian‐Type Basis Sets for Lithium, Beryllium, and Boron, *J. Chem. Phys.*, 1975, **62**, 2921.

9 M. M. Francl, W. J. Pietro, W. J. Hehre, J. S. Binkley, M. S. Gordon, D. J. DeFrees and J. A. Pople, Self‐Consistent Molecular Orbital Methods. XXIII. A Polarization‐Type Basis Set for Second‐Row Elements, *J. Chem. Phys.*, 1982, **77**, 3654.

10 W. J. Hehre, R. Ditchfield and J. A. Pople, Self-Consistent Molecular Orbital Methods. XII. Further Extensions of Gaussian-Type Basis Sets for Use in Molecular Orbital Studies of Organic Molecules, *J. Chem. Phys.*, 1972, **56**, 2257.

11 M. Dolg, P. Pyykkö and N. Runeberg, Calculated Structure and Optical Properties of $Tl_2Pt(CN)_4$, *Inorg. Chem.*, 1996, **35**, 7450.

12 R. E. Stratmann, G. E. Scuseria and M. J. Frisch, An Efficient Implementation of Time-Dependent Density Functional Theory for the Calculation of Excitation Energies of Large Molecules, *J. Chem. Phys.*, 1998, **109**, 8218.

13 M. E. Casida, C. Jamorski and K. C. Casida, Molecular Excitation Energies to High-Lying Bound States from Time-Dependent Density-Functional Response Theory: Characterization and Correction of the Time-Dependent Local Density Approximation Ionization Threshold, *J. Chem. Phys.*, 1998, **108**, 4439.

14 R. Bauernschmitt and A. Ahlrichs, Treatment of Electronic Excitations within the Adiabatic Approximation of Time Dependent Density Functional Theory, *Chem. Phys. Lett.*, 1996, **256**, 454.

15 T. Lu and F. Chen, Multiwfn: A Multifunctional Wavefunction Analyzer, *J. Comput. Chem.*, 2012, **33**, 580.

16 J. M. Younker and K. D. Dobbs, Correlating Experimental Photophysical Properties of Iridium(III) Complexes to Spin–Orbit Coupled TDDFT Predictions, *J. Phys. Chem. C*, 2013, **117**, 25714.

17 R. A. Boto, F. Peccati, R. Laplaza, C. Quan, A. Carbone, J.-P. Piquemal, Y. Maday and J. Contreras-Garcia, NCIPLOT4: Fast, Robust, and Quantitative Analysis of Noncovalent Interactions, *J. Chem. Theory Comput.* 2020, **16**, 4150.

18 J. Contreras-Garcia, E. R. Johnson, S. Keinan, R. Chaudret, J.-P. Piquemal, D. N. Beratan and W. Yang, NCIPLOT: A Program for Plotting Noncovalent Interaction Regions, *J. Chem. Theory Comput.*, 2011, **7**, 625.

19 E. R. Johnson, S. Keinan, P. Mori-Sánchez, J. Contreras-García, A. J. Cohen and W. Yang, Revealing Noncovalent Interactions, *J. Am. Chem. Soc*., 2010, **132**, 6498.

20 W. Humphrey, A. Dalke and K. Schulten, VMD: Visual Molecular Dynamics, *J. Mol. Graphics*, 1996, **14**, 33.

21 P. Jonkheijm, P. van der Schoot, A. P. Schenning and E. W. Meijer, Probing the Solvent-Assisted Nucleation Pathway in Chemical Self-Assembly, *Science*, 2006, **313**, 80.

22 M. Toumi, F. Couty and G. Evano, Total Synthesis of Paliurine F, *Angew. Chem. Int. Ed.*, 2007, **46**, 572.

23 (a) R. L. J. Victo, Bloemendal, D. Sondag, H. Elferink, T. J. Boltje, J. C. M. van Hest and F. P. J. T. Rutjes, A Revised Modular Approach to (–)-*trans*-Δ^8-THC and Derivatives Through Late-Stage Suzuki–Miyaura Cross-Coupling Reactions, *Eur. J. Org. Chem.*, 2019, 2289. (b) Y. Ito, Y. Haketa, N. Eifuku, E. Lee, M. Lee, T. Hashishin, K. Kaneko and H. Maeda, Solvent-Assisted Organized Structures Based on Amphiphilic Anion-Responsive π-Conjugated Systems, *Chem. Eur. J.*, 2009, **15**, 3706. (c) C. Po and V. W.–W. Yam, A Metallo-Amphiphile with Unusual Memory Behaviour: Effect of Temperature and Structure on the Self-Assembly of Triethylene Glycol (TEG)–Pendant Platinum(II) Bzimpy Complexes, *Chem. Sci.*, 2014, **5**, 4868.

24 S. Schlamp, P. Thoma and B. Weber, Head–Tail Iron(II) Complexes with Spin Crossover Properties, *Eur. J. Inorg. Chem.*, 2012, 2759.

25 C. H. Jani, C. H. Lalander, S. J. Langford, I. Nerush, J. Shapter, D. Villamaina, E. Vautheyc and S. V. Bhosale, Supramolecular Construction of Vesicles Based on Core-Substituted Naphthalene Diimides Bearing TEG Motifs, *Chem. Commun*., 2011, **47**, 8226.

26 J. Li, F. Song, L. Wang, J. Jiao, Y. Cheng and C. Zhu, Excitation Induced Emission Color Change Based on Eu(III)-Zn(II)-containing Polymer Complex, *Macromol. Rapid Commun.*, 2012, **33**, 1268.